DASA-2718

February 15, 1971

DYNAMIC SHEAR STRENGTH OF SHOCK-LOADED GRANITE AND POLYCRYSTALLINE QUARTZ

Final Report

By

J. T. ROSENBERG

HEADQUARTERS
DEFENSE NUCLEAR AGENCY
WASHINGTON, D.C. 20305

STANFORD RESEARCH INSTITUTE
MENLO PARK, CALIFORNIA 94025

DASA 01-69-C-0073

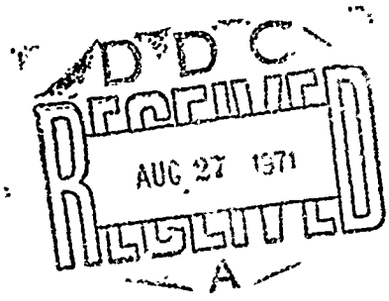

Final Report

DASA-2718

February 15, 1971

DYNAMIC SHEAR STRENGTH OF SHOCK-LOADED GRANITE AND POLYCRYSTALLINE QUARTZ

By: J. T. ROSENBERG

Prepared for:

DEFENSE ATOMIC SUPPORT AGENCY
WASHINGTON, D.C. 20305
Attention: MR. C. B. McFARLAND
SHOCK PHYSICS DIRECTORATE

CONTRACT DASA 01-69-C-0073

SRI Project PYU 7852

This work was supported by the Defense Nuclear Agency under NWER Subtask S8047.

Approved by:

GEORGE R. ABRAHAMSON, *Director*
Poulter Laboratory

C. J. COOK, *Executive Director*
Physical Sciences Division

UNCLASSIFIED

Security Classification

DOCUMENT CONTROL DATA - R & D

Security classification of title, body of abstract and indexing annotation must be entered when the overall report is classified)

1 ORIGINATING ACTIVITY (Corporate author)

Stanford Research Institute
333 Ravenswood Avenue,
Menlo Park, California 94025

2a. REPORT SECURITY CLASSIFICATION

UNCLASSIFIED

2b. GROUP

3 REPORT TITLE

DYNAMIC SHEAR STRENGTH OF SHOCK-LOADED GRANITE AND POLYCRYSTALLINE QUARTZ

4. DESCRIPTIVE NOTES (Type of report and inclusive dates)

Final Report (April 1, 1969 through April 15, 1971)

5. AUTHOR(S) (First name, middle initial, last name)

John T. Rosenberg

6 REPORT DATE	7a. TOTAL NO OF PAGES	7b. NO OF REFS
February 15, 1971	84	36

8a. CONTRACT OR GRANT NO.	9a. ORIGINATOR'S REPORT NUMBER(S)
DASA01-69-C-0073	SRI PYU 7852
b. PROJECT NO.	
c. Subtask SB047	9b. OTHER REPORT NO(S) (Any other numbers that may be assigned this report)
d.	DASA 2718

10. DISTRIBUTION STATEMENT

Approved for public release; distribution unlimited.

11. SUPPLEMENTARY NOTES	12. SPONSORING MILITARY ACTIVITY
	Director, Defense Nuclear Agency Washington, D. C. 20305

13. ABSTRACT

Shock wave experiments were conducted to determine the behavior of the dynamic shear strength near the Hugoniot elastic limit (HEL) for two low-porosity silicate rocks. The materials studied were Westerly granite and Arkansas novaculite. The HEL of dry novaculite was found to be 55-60 kbar at 100 kbar peak stress, and that of dry granite was 30 kbar at 60 kbar peak stress, as determined using multiple in-material manganin stress transducers. Examination of a recovered dry granite specimen shocked to 50 kbar and released in uniaxial strain revealed it to have well cemented grain boundaries, extensive random microcracks crossing the grain boundaries, and no planar features. Several significant new results were obtained in this program. The HEL of dry granite was found to be insensitive to variations in microcrack density and shock-loading rate over the ranges of variation investigated. The unloading response of dry granite from stresses above the HEL is apparently initially elastic. An unexpectedly large decrease was observed in the HEL of granite when it was fully saturated with water prior to shock loading. These results have allowed us to suggest a mechanism for the internal processes occurring at the HEL. The major feature of the proposed yielding mechanism is that by totally filling all connected microcracks with water, we have constrained these cracks to remain open during shock loading. In this configuration they can support only a negligible shear stress as compared to evacuated microcracks which can close and friction-lock during shock compression.

DD FORM 1 NOV 68 1473 (PAGE 1)

S/N 0101-807-6801

UNCLASSIFIED

Security Classification

14 KEY WORDS	LINK A		LINK B		LINK C	
	ROLE	WT	ROLE	WT	ROLE	WT
Dynamic Shear Strength						
Hugoniot Elastic Limit						
Fracture						
Shock Propagation						
Granite						
Water-saturated Granite						

ABSTRACT

Shock wave experiments were conducted to determine the behavior of the dynamic shear strength near the Hugoniot elastic limit (HEL) for two low-porosity silicate rocks. The materials studied were Westerly granite and Arkansas novaculite. The HEL of dry novaculite was found to be 55-60 kbar at 100 kbar peak stress, and that of dry granite was 30 kbar at 60 kbar peak stress, as determined using multiple in-material manganin stress transducers. Examination of a recovered dry granite specimen shocked to 50 kbar and released in uniaxial strain revealed it to have well cemented grain boundaries, extensive random microcracks crossing the grain boundaries, and no planar features.

Several significant new results were obtained in this program. The HEL of dry granite was found to be insensitive to variations in microcrack density and shock-loading rate over the ranges of variation investigated. The unloading response of dry granite from stresses above the HEL is apparently initially elastic. An unexpectedly large decrease was observed in the HEL of granite when it was fully saturated with water prior to shock loading. These results have allowed us to suggest a mechanism for the internal processes occurring at the HEL. The major feature of the proposed yielding mechanism is that by totally filling all connected microcracks with water, we have constrained these cracks to remain open during shock loading. In this configuration they can support only a negligible shear stress as compared to evacuated microcracks which can close and friction-lock during shock compression.

ACKNOWLEDGMENTS

I would like to acknowledge and thank Dr. Donald Grine of the Stanford Research Institute and Dr. William Nix of the Materials Science Department, Stanford University, for their suggestions and criticisms which were extremely helpful throughout the course of this work. For specific contributions without which this project could not have been successfully completed, I would like to express my appreciation and gratitude to the following: Mr. R. W. Gates for preparing and characterizing the granite specimens, Dr. Lynn Seaman for performing the PUFF code simulations of laminated projectile impact experiments, Mr. Paul De Carli for his help with the uniaxial strain granite recovery experiment, Dr. Howard Wilshire of the U.S. Geological Survey, Menlo Park, California for looking at the shocked and recovered granite thin section, Miss Courtney Soule of Stanford University for petrographic descriptions of our granite specimens, Dr. David Wones, Department of Geophysics, Massachusetts Institute of Technology for obtaining specimens of granite for us from quarries near Westerly, Rhode Island, Dr. Wayne Brown, Mechanical Engineering Department, University of Utah for furnishing us a sample of the granite on which triaxial tests were performed in his laboratory, and Mr. E. H. Southard, Manager of the Norton Pike Division, Littleton, New Hampshire, for selecting Arkansas novaculite specimens to our requirements.

CONTENTS

LIST OF FIGURES

I INTRODUCTION

During the past decade considerable effort has been exerted toward understanding and predicting the propagation in the earth of large amplitude stress waves, such as those generated by chemical and nuclear explosives or by impact of extraterrestrial bodies. Although progress has been made, it is not yet possible to predict the entire flow resulting even from a planned and controlled energy release experiment in the earth. In particular, the two-dimensional computer code simulations of nuclear events in hard rocks (e.g., PILE DRIVER) are substantially in error in their estimates of both far-field particle displacements and intermediate station flow stresses.[1]

Since the accuracy of such code simulations is limited both by the validity of the rheological model being used and by the precision to which the input parameters are known, experimental programs have been undertaken at SRI[2-5] and other laboratories[1, 6-13] to evaluate the constitutive relations which characterize hard rocks in the codes. In the present research program we examined the dynamic shear strength (as defined by the Hugoniot elastic limit, HEL) and the dynamic unloading behavior of hard rocks, since neither had been well determined and since the results of code calculations are sensitive to both. The specific objectives of this program were (1) to determine the dependence of the HEL of typical hard rocks on initial specimen state and loading rate and (2) to obtain shock-loading and unloading data for these rocks.

Arkansas novaculite, a fine-grained naturally occurring polycrystalline quartz, and Westerly granite were selected as the study materials. These materials were shock loaded using either the SRI $2\frac{1}{2}$-inch[14] or the 4-inch light gas gun. In most experiments the specimens were instrumented with multiple in-material manganin stress transducers, and the resulting stress-time data were reduced using Lagrangian data analysis methods. These methods allow release paths to be measured without making the restrictive and perhaps invalid assumptions on the nature of the release process (such as that it is isentropic) that were required in previous investigations. Two recovery experiments were also performed to permit examination of material shocked above the HEL.

Section II of this report is a summary of the results and conclusions of the present investigation. Section III describes the shock wave theory and terminology relevant to measuring the shock strength and unloading behavior of hard rocks and includes a discussion of stress transducers and Lagrangian data analysis. Section IV is a detailed presentation of the experimental methods and results, and in Section V we discuss our conclusions.

II SUMMARY

The major results of this investigation are:

(1) The HEL of Arkansas novaculite shocked to about 100-kbar peak stress is 55-60 kbar.

(2) The elastic Hugoniot of novaculite is well represented for wave propagation calculations by a linear σ_x-V relation.

(3) The HEL of dry Westerly granite shocked to 60 kbar is about 30 kbar.

(4) The HEL of dry Westerly granite is independent of (a) changes in microcrack density caused by uniaxial stress-induced dilatancy and (b) a decrease in shock-loading rate of about 1/3.

(5) The HEL, and hence the dynamic shear strength, of Westerly granite becomes too low to be measured in our experiments when the granite is fully saturated with water.

(6) The initial release of dry, shock-loaded Westerly granite is nearly elastic.

(7) Recovered samples of Westerly granite shocked above the HEL have well-cemented grain boundaries, are covered with a mosaic of microfractures, and exhibit no planar features.

(8) We have proposed a model for the microscopic plastic process occurring at the HEL.

Of these results, the most surprising and significant are (4)-(7), and in particular (5), that fully saturating granite with water causes the HEL to become negligibly small compared to that of the same granite dry. It is these observations which provide the basis for the microscopic model (8) which we have suggested.

III TECHNICAL BACKGROUND

A. Shock-Wave Relations for an Ideal Elastic-Plastic Hard Rock

The Rankine-Hugoniot relation [Hugoniot], sometimes known as the shock adiabat, is the locus of final equilibrium states that a material can attain from a given initial state as a result of loading by a plane, steady-state shock wave. The Hugoniot is usually specified by giving the axial component of the stress tensor (the major principal stress) as a function of some strain variable such as specific volume or volumetric strain (which is equal to axial strain for plane shock-wave geometry). Alternatively for steady-state flow (no time dependence), one can use the two Rankine-Hugoniot jump conditions[15] which express the conservation of mass and momentum to convert the Hugoniot from the stress-strain plane to any of the six possible planes defined by the four flow variables: stress, strain, shock velocity, and particle velocity. The Hugoniot is the constitutive relation, or partial equation of state, which, because of its relative ease of measurement, is most often used to characterize earth materials in the stress range above about 100 kbar where strength effects are assumed to be negligible.

The Hugoniot, and all shock-wave experiments performed on this program, pertain to uniaxial strain. There may be local instabilities in the flow, caused for example by specimen flaws, at which this condition is temporarily violated. However, the lateral boundary conditions and locations, and the specimen homogeneity and isotropy in planes normal to the flow ensure that the constraint holds macroscopically.

In plane shock-wave experiments, it is usually assumed that the initial mechanical loading response of a nonporous hard rock is elastic. During this phase of loading as the axial stress associated with the shock front increases, the specimen develops a radial stress of the magnitude required to maintain uniaxial strain. The difference between these two represents a shear stress, or stress deviator, which increases as the shock amplitude increases. When the stress deviator exceeds the specimen shear strength, a stress-relieving process, which we shall refer to as plastic flow, occurs. The further response of the rock specimen to additional loading is

characterized as plastic. The axial stress at the elastic limit is known as the Hugoniot elastic limit (HEL).

After compression, the rock is unloaded by a stress relief or rarefaction wave. This rarefaction must originate at a free surface oriented perpendicular to the direction of uniaxial flow to maintain the 1-D geometry during unloading. For an ideal elastic-plastic material, the initial unloading will be elastic. That is, as the axial stress is reduced by the rarefaction, the stress deviator can decrease and cease to drive plastic flow. However, in analogy to the compression process, as unloading continues the stress deviator continues to decrease until it again becomes large enough in the negative direction to cause plastic flow. These concepts are illustrated in Fig. 1, which shows the Hugoniot and release path in stress-specific volume space for an idealized hard rock. Also shown is the Rayleigh line,[15] the locus of actual σ_x-V states which the mass elements experience while being shock loaded to a given Hugoniot state, and the hydrostat, the locus of stress-specific volume states attained under hydrostatic compression, i.e., with $\sigma_x = \sigma_y = \sigma_z$. In shock-wave calculations, the assumption is usually made that after thermal corrections, the hydrostat gives the mean stress, $(\sigma_x + \sigma_y + \sigma_z)/3$, at a given specific volume for any applied stress configuration and, in particular, for the idealized uniaxial strain cycle of Fig. 1 Whereas the Hugoniot is the locus of final states which can be reached by various amplitude shocks but is not the path actually followed in a shock compression, the release path, Rayleigh line, and hydrostat in Fig. 1 each represent states actually occupied during the shock-release cycle.

Note in Fig. 1 that, after the axial stress has been reduced to zero, a volume compression and hence a nonzero mean stress remain. In a shock-wave experiment these are reduced later by rarefactions propagating into the specimen from the lateral boundaries. Because of these lateral rarefactions in even an ideal shock-wave recovery experiment, it is impossible to avoid some lateral flow. This lateral flow may significantly affect interpretation of features observed in recovered specimens.

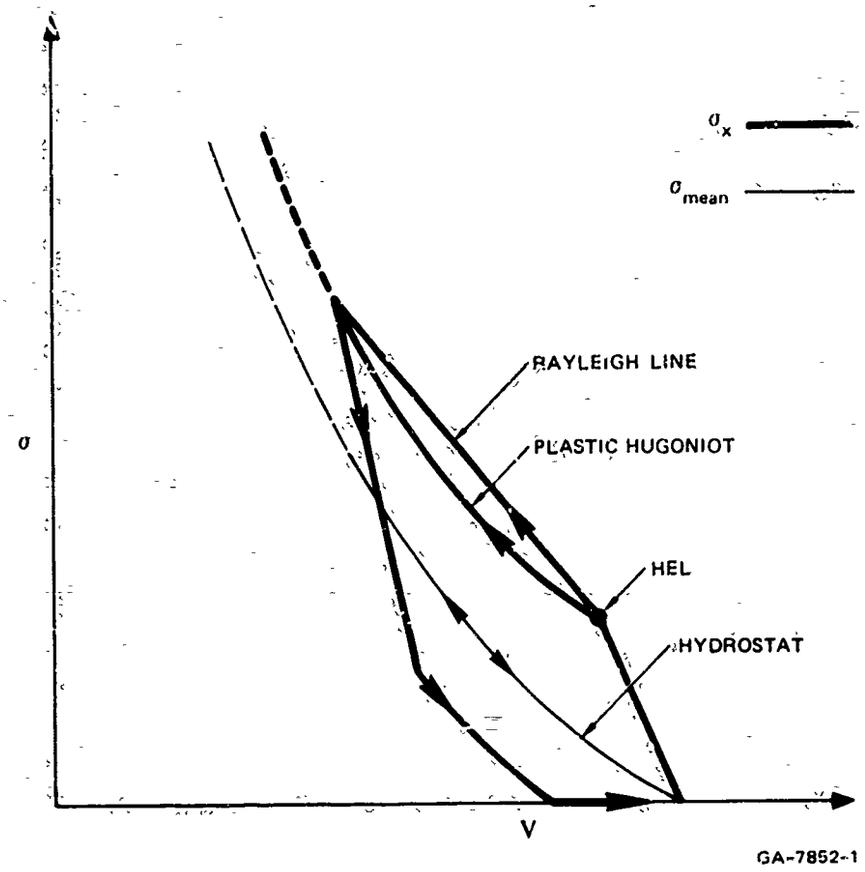

FIGURE 1 **STRESS-SPECIFIC VOLUME RESPONSE OF AN IDEAL HARD ROCK (SIMPLE ELASTIC-PLASTIC) DURING A UNIAXIAL STRAIN LOAD-RELEASE CYCLE.** The arrows indicate the direction these paths follow during the cycle. Note that below the HEL the Rayleigh line and the elastic Hugoniot coincide.

What is the rheological response to plane shock loading of a material having the idealized mechanical properties represented by Fig. 1 ? For shocks of amplitude less than the HEL, a simple shock front referred to as the elastic precursor propagates through the specimen. For the linear elastic response shown in Fig. 1, the precursor travels with the stress-independent longitudinal elastic velocity which may be evaluated from Fig. 1 using the well-known relation[15]

$$C^2 = -V^2\left(\frac{d\sigma_x}{dV}\right).$$

For shock amplitudes greater than the HEL, a single front is not stable;[16] and the shock separates into an elastic precursor traveling with velocity C and a slower plastic wave whose velocity U may be calculated using the Rankine-Hugoniot jump conditions[15] if the flow is steady (no time dependence). This separation of the loading wave into multiple fronts occurs not only at the HEL, but whenever the σ_x-V Hugoniot has a discontinuous increase in slope with increasing σ (if the second derivative of the Hugoniot with respect to volume does not become positive) such as at a first-order, time-independent phase transformation to a denser phase.

The rarefaction which unloads the specimen also separates for a material having the mechanical response modeled in Fig. 1. The initial unloading pulse is elastic and again travels into the material ahead with velocity C. The slower plastic unloading pulse spreads with time since each incremental rarefaction travels at stress-dependent velocity $C(\sigma_x)$, where for a particular $\sigma_x = \sigma_x'$

$$C(\sigma_x') = -V^2 \left(\frac{d\sigma_x}{dV}\right)_{\sigma_x'}$$

For a rarefaction originating on the same side of the specimen as the shock (from the back surface of a projectile head), the entire stress pulse at some instant of time for the load-release cycle of Fig. 1 is shown in Fig. 2. In Fig. 2, spreading effects in the rarefaction due to mass flow are ignored.

For real materials (1) the elastic-plastic transition usually does not occur at a single stress (the Hugoniot usually is curved, not just "kinked" at the HEL), (2) there are transient effects which do not disappear until the flow becomes steady, (3) there are complex finite elastic deformational and inelastic material processes occurring during both the so-called elastic and plastic phases of loading, and (4) there are thermal effects due to the irreversibility of the shock process itself, all of which cause deviations from the idealized behavior modeled in Figs. 1 and 2.

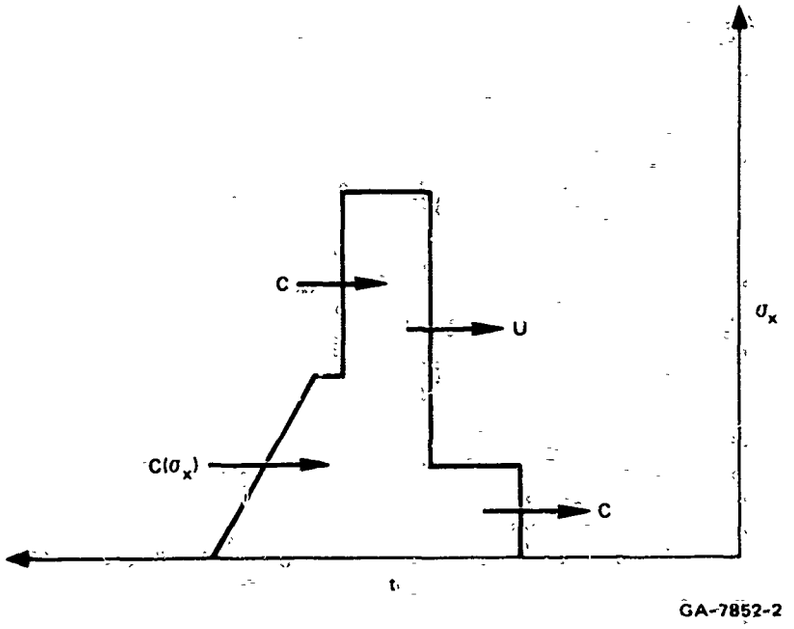

FIGURE 2 AXIAL STRESS-TIME PROFILE SEEN BY A MASS ELEMENT DURING THE LOAD-RELEASE CYCLE OF FIGURE 1

B. Lagrangian Analysis

For real flows which are not in general steady or isentropic, the shock wave data analysis techniques which are usually used, the Rankine-Hugoniot jump conditions for calculating Hugoniot states and the Riemann invariant[15] for calculating release states, are not valid. However, the average axial stress-specific volume states achieved both in compression and release by a mass element at some point in the flow may still be calculated using the Lagrangian gage method suggested independently by Fowles at Physics International and Williams at SRI.[17] The analysis has recently been further developed by Cowperthwaite and Williams.[18]

For a general flow, the stress-gage version of this technique requires correlated stress-time records to be obtained at a minimum of three points in the flow. Figure 3 schematically shows a typical Lagrangian gage configuration with three vertically stacked in-material gages. From the resulting stress records, we calculate C_σ, the velocity with which constant

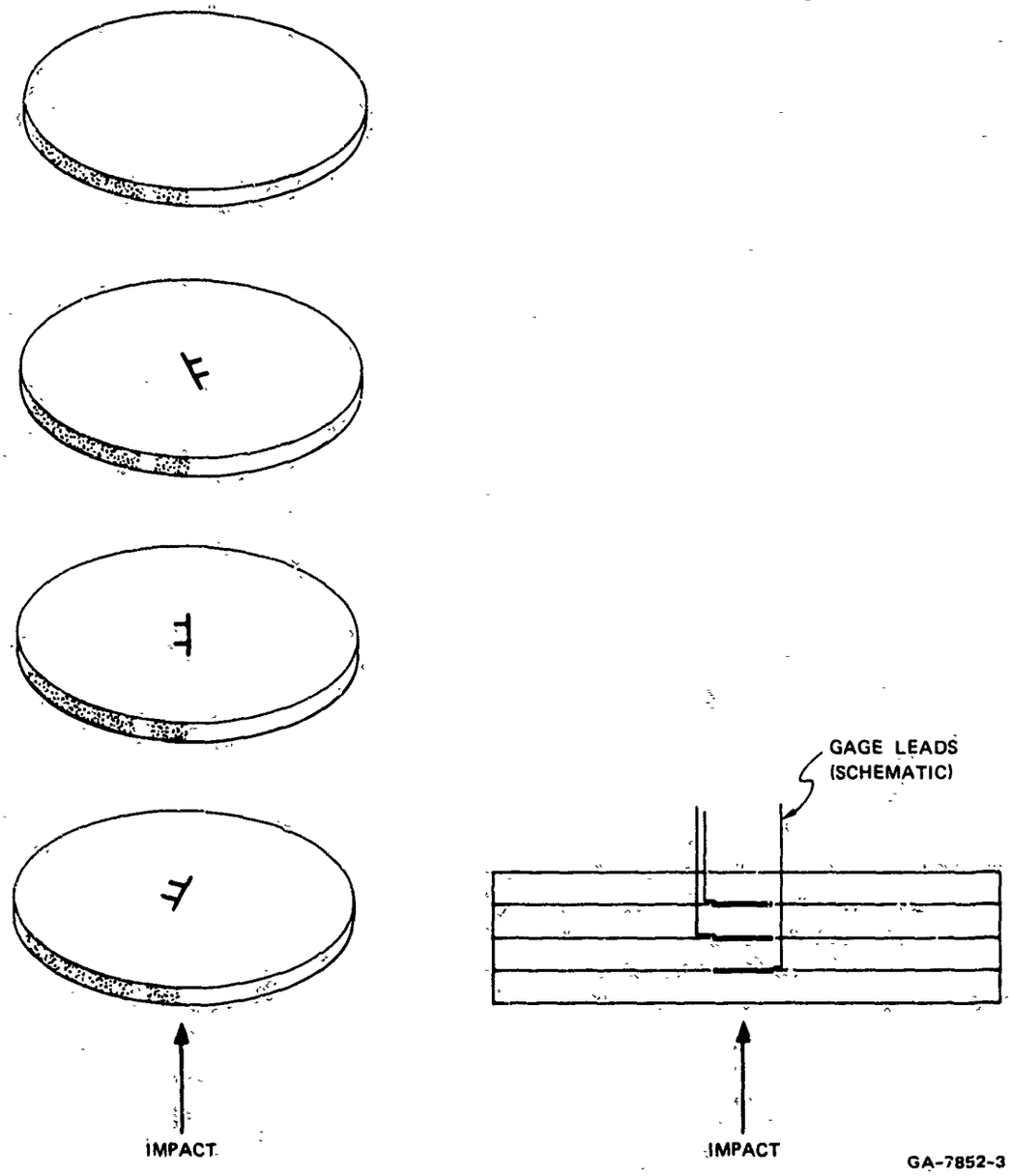

FIGURE 3 TYPICAL LAGRANGIAN GAGE CONFIGURATION, EXPLODED AND SIDE VIEWS. Note that the four terminal π gages are rotated with respect to each other so that the leads from one gage will not interfere with those from another when they are brought out the back of the target. If the leads are brought out the sides in the lamination planes, this rotation is not necessary.

stress elements of the flow propagate in Lagrangian coordinates (the velocity with which these elements propagate from one gage to the next in a reference frame in which the coordinate system moves with the gages). The values of C_σ are used to integrate the differential flow equations expressing the conservation of mass and momentum, according to the scheme described by Cowperthwaite and Williams. No assumptions on the nature of the flow are made other than that it is uniaxial, however, accuracy is dependent upon the number of gage stations at regions in which C_σ is a strongly varying function of Lagrangian position. At least three gage positions, defining two measurement intervals, are required to observe the dependence, if any, of C_σ on position.

The σ_x-V states calculated using the Lagrangian analysis are analogous to the Rayleigh line and release path of Fig. 1. That is, they represent the actual states traversed by a mass element during compression and release, the loading and unloading paths. In the event that the flow is a steady-state compression or an isentropic release, they are readily shown[17,18] to correspond precisely to the Rayleigh line and isentrope represented in Fig. 1.

If the flow is not steady, the technique is still applicable; however, it is not exact since C_σ is approximated in the interval between two gage positions by its average value in that interval. It is for this reason that the σ_x-V path so calculated is said to represent a material average. It is an estimate of the states achieved by a mass element near the "middle" of the three-gage interval. (For a steady flow, all mass elements pass through the same states, of course.) One of the purposes of the present research program is to obtain compression and release paths for hard rocks shocked to near the HEL without making the assumptions on the nature of the flow which were necessary before stress-gage technology was improved and the Lagrangian analysis methods were developed.

IV EXPERIMENTS AND RESULTS

A. Arkansas Novaculite

Arkansas novaculite is a naturally occurring form of very fine grained polycrystalline quartz. Specimens used in the present program were obtained from the Norton Company, Littleton, New Hampshire and have previously been described[19] as homogeneous, isotropic, nearly nonporous, with an average grain size of ~0.01 mm and a silica content of greater than 99%. Novaculite was selected for study because (1) among silicate rocks its uniformity and small grain size make it one of the most likely to yield reproducible shock wave data, and (2) it is basically monomineralic (SiO_2), and therefore may provide insight into the fracture mechanisms in more complex silicate rocks such as granites.

Four shock experiments were performed using novaculite targets. In two of these the shock amplitude was less than the HEL and information was obtained on the elastic portion of the Hugoniot and on the feasibility of using laminated head projectiles to generate reduced strain-rate dynamic loading data. In the other two experiments, novaculite was shocked to higher final stresses to allow measurements of the HEL and of the effects on the HEL of underlying gage plane cracks and inclusions in the specimen. The two shots in which novaculite was shocked below its HEL are discussed first.

The laminated-head $2\frac{1}{2}$-inch gas gun projectile shown in Fig. 4 was designed to provide strain rates about an order of magnitude less than are obtained in conventional gas gun experiments on hard rocks. The components of the projectile head starting from the impact surface are: (1) ~0.5 mm foam, composed of phenolic microballoons and C-7 epoxy, fabricated at SRI to a uniform density of 0.50 g/cm^3, (2) ~0.5 mm of C-7 epoxy, ρ_o = 1.18 g/cm^3, (3) ~ 1 mm of 2024 Al, and (4) ~ 13 mm of high lead brass. Both faces of each laminate were machined flat and parallel to within 0.001 inch (.025 mm) and these tolerances were maintained during assembly. As shown in Fig. 4, the first three laminates were of slightly smaller diameter than the fourth (brass) laminate and projectile body so that these latter would provide both a good reference surface and electrical

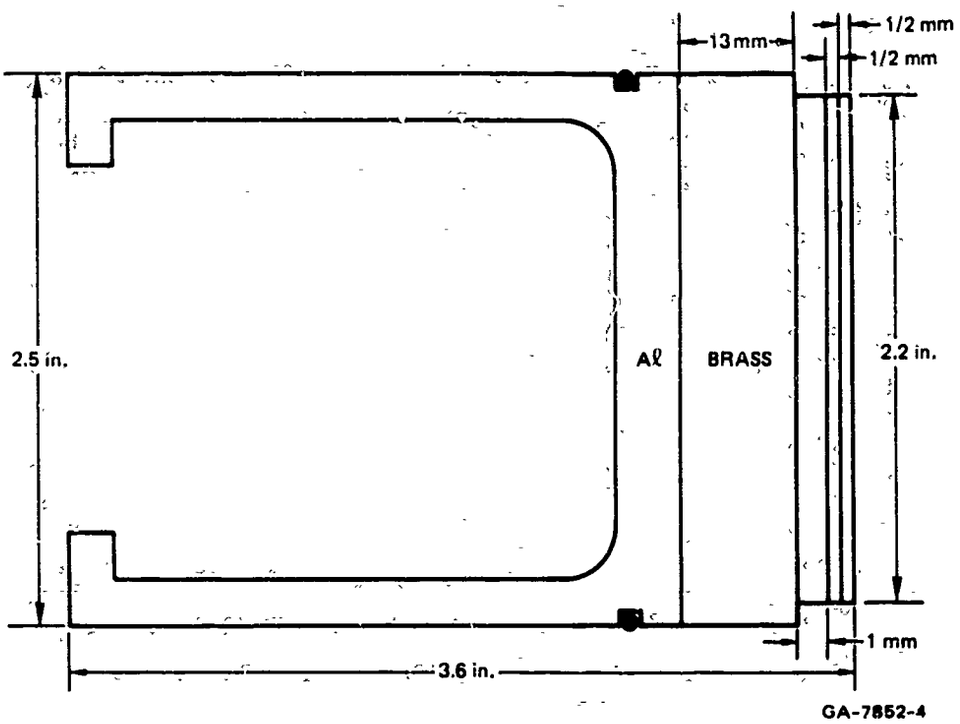

FIGURE 4 LAMINATED-HEAD PROJECTILE FOR 2½-INCH GAS GUN. The three thin laminate layers starting from the impact side are an epoxy-microballoon foam, C-7 epoxy, and 2024-Al, respectively

continuity to the gun barrel as required for projectile velocity measurement. The choice of laminate materials and thicknesses was checked and optimized using SRI PUFF,[20] a one-dimensional artificial viscosity computer code.

The stress record obtained using a conventional 4-terminal manganin foil gage[21] embedded ~1 mm into novaculite from the impact surface is shown in Fig. 5. In this experiment (Shot 908) the projectile velocity was 0.62 mm/μsec. The peak stress in novaculite was 64 kbar calculated from the manganin piezoresistive coefficient reported by Keough[21] of $0.29 \times 10^{-2} \frac{\Delta R/R}{\text{kbar}}$, where R is the resistance of the gage element prior to shock loading and ΔR is shock-induced change in resistance. The rise time of the compression wave is ~0.6 μsec, 5 to 60 kbar, with shock planarity

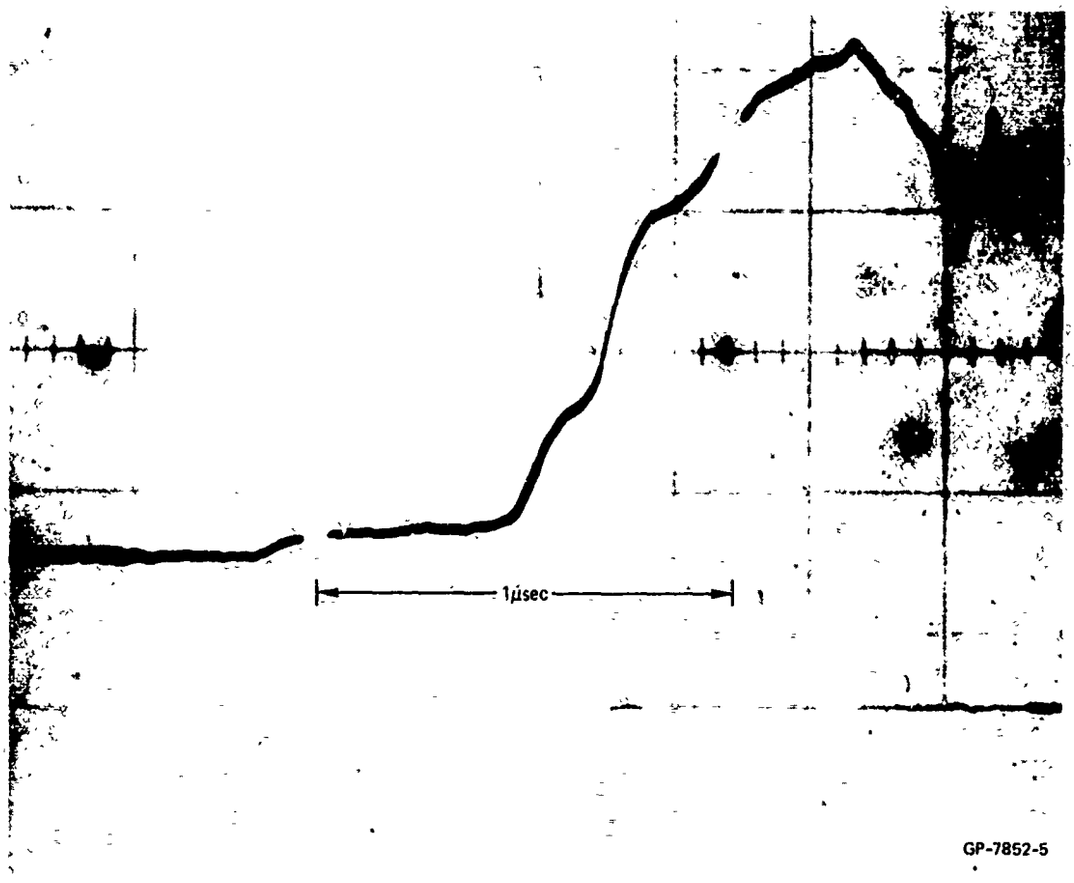

FIGURE 5 MANGANIN GAGE RECORD 4 mm INTO NOVACULITE GENERATED BY LAMINATED PROJECTILE OF FIGURE 3 TRAVELING AT 0.6 mm/μsec, SCOPE 29, SHOT 908. The structure at the end of the record is the gage failure signal; it does not reflect the actual stress in the novaculite.

across the gage <0.1 μsec. For comparison, the stress profile 6 mm into novaculite predicted by PUFF for a projectile velocity of 0.8 mm/μsec is shown in Fig. 6. The significance of the good agreement between the stress profiles of Figs. 5 and 6 is discussed in Section V.

In Shot 909 another laminated head projectile was impacted into a novaculite target fronted with a 3-mm thick disk of 70% dense tungsten foam. The purpose of the tungsten foam was to generate a smoother stress-time loading profile than that obtained in Shot 908 (Fig. 5). However, the tungsten foam actually caused the low stress portion of the compression pulse to spread and the high stress portion to shock up, as can be seen from the manganin gage record in Fig. 7.

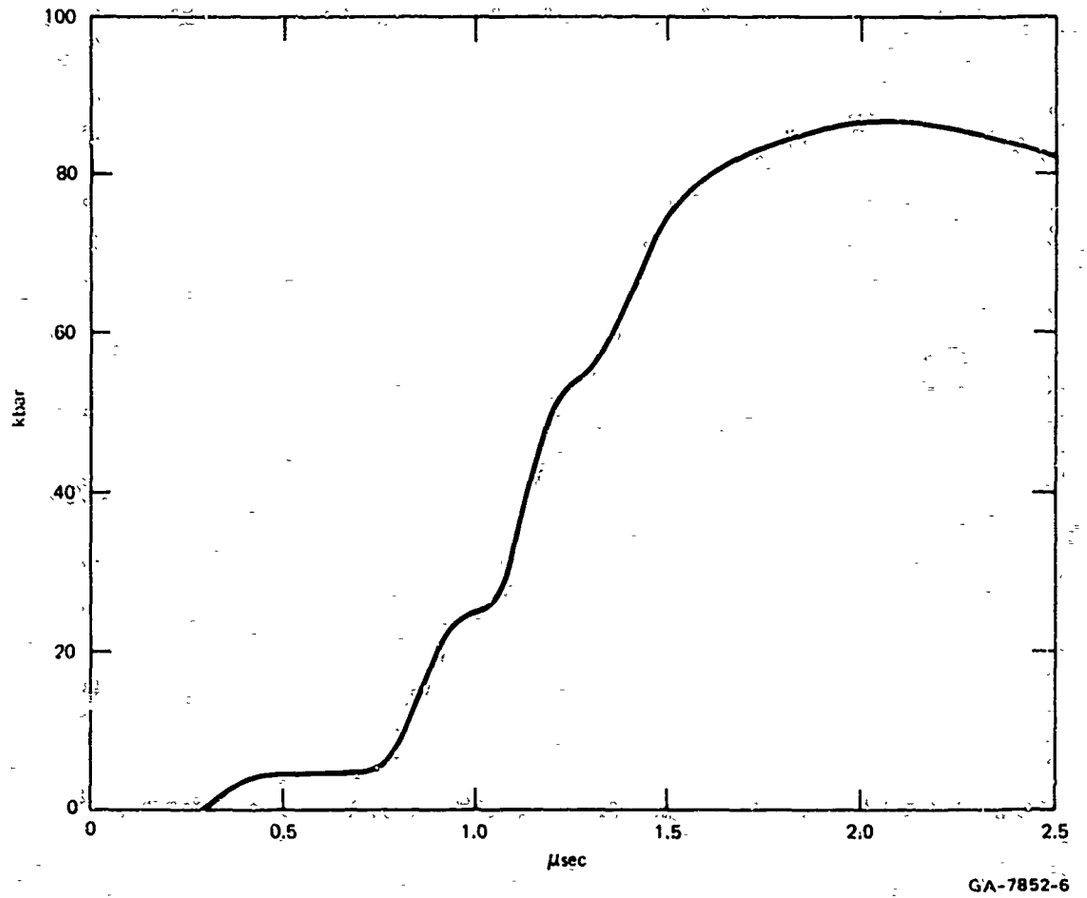

FIGURE 6 PUFF PREDICTION OF STRESS PROFILE 6 mm INTO NOVACULITE GENERATED BY LAMINATED PROJECTILE OF FIGURE 3 TRAVELING AT 0.8 mm/μsec. Small, high-frequency oscillations in g, generated internally by PUFF, were present for the first 0.4μsec but are not shown here, as they could be eliminated by refining the mesh size.

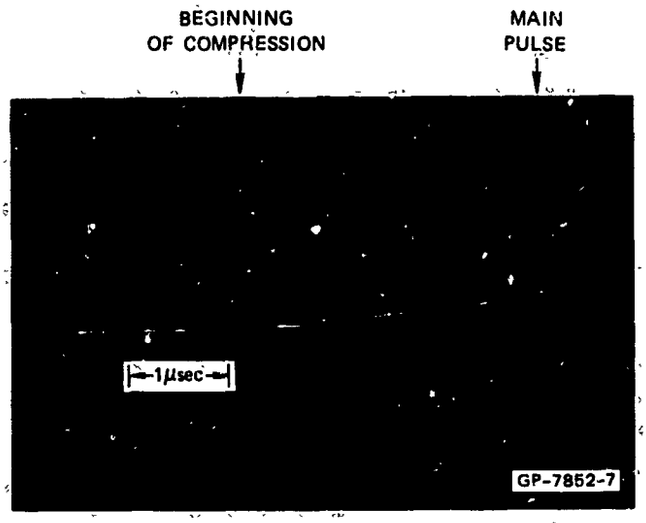

FIGURE 7 MANGANIN GAGE RECORD OF STRESS PROFILE 4 mm INTO NOVACULITE FRONTED WITH 3 mm OF TUNGSTEN FOAM AND IMPACTED AT 0.6 mm/μsec BY THE LAMINATED PROJECTILE OF FIGURE 3, SCOPE 23, SHOT 909. The structure at the end of the main pulse is the gage failure signal; it is not part of the loading pulse.

For a projectile velocity of 0.63 mm/μsec, the rise time of the 0 to 20% maximum stress signal is approximately 2.5 μsec and that of the 20-90% peak stress signal is about 0.1 μsec. Although the profile in novaculite is indeed smoother in Shot 909 than in Shot 908 (see Figs. 5 and 7), the strain rate is significantly lower only during the initial phases of loading and not at higher stresses near the HEL. On the basis of Shots 908 and 909, we concluded that laminated projectiles do not generate sufficiently uniform loading to allow resolution of the HEL. For our subsequent reduced strain rate loading experiments in granite, we used a fused quartz front disk on the target to spread the shock the desired amount in the manner suggested by Barker and Hollenbach.[22] This technique cannot be applied to novaculite with its high HEL, because fused quartz is dispersive only below about 40 kbar.

The two experiments in which the HEL of novaculite was exceeded were also fired on the 2½-inch light gas gun. To reach the stresses required in these experiments, we used a lightened 7075 Al projectile body with internal ribs for additional strength and a swaged-in brass head for high shock impedance. These projectiles weigh approximately 230 g, support 6000 psi laterally in the gas gun breech, and reach a velocity of ~1 mm/μsec.

Previous determinations of the novaculite HEL,[19,23] made using inclined mirrors to monitor free surface motion and the free surface velocity approximation[15,23] for data reduction, have yielded a range of values from 40 to 140 kbar for peak pressures from 100 to 400 kbar. The purpose of the first high velocity shot (Shot 970) was to observe the profile of the novaculite precursor and measure its amplitude for a peak stress of about 100 kbar.

In Shot 970 the light weight projectile impacted a 1/4-inch thick novaculite target backed with a thick C-7 epoxy disk containing a manganin wire stress transducer 2 mm from the novaculite C-7 interface. A classic two-wave profile was recorded in the C-7 as shown in Fig. 8. The amplitude of the precursor was 25 kbar and that of the main wave was 47 kbar, both in C-7. These figures correspond to a 60-kbar HEL in novaculite driven by a 100-kbar main wave. Projectile velocity was 0.97 mm/μsec. Rise times are not reported since they are strongly dependent on the wave propagation properties of C-7.

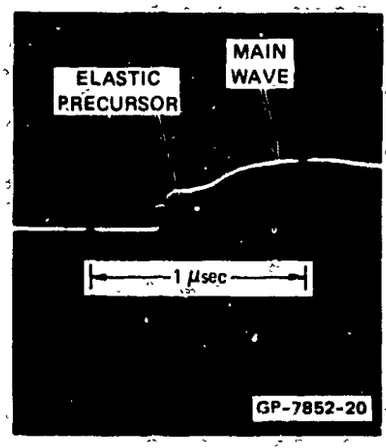

FIGURE 8 STRESS PROFILE OBSERVED IN C-7 MANGANIN GAGE PACKAGE MOUNTED ON ¼-INCH THICK NOVACULITE TARGET SHOCKED TO 100 kbar, SHOT 970, SCOPE 30

In Shot 982 the same type projectile impacted a novaculite target containing three manganin foil gages. Figure 9 is a side view drawing of the target showing the relative positions of the three gage elements. The objectives of this shot were to measure precursor rise times, to observe the HEL directly, and to determine the effects of underlying cracks and gage elements on subsequent flow. Referring to Fig. 9, one sees that gage 1 records the intrinsic HEL 9 mm into novaculite, gage 2 sees the precursor after it has passed over and interacted with gage 1 and traveled an additional 5 mm, and gage 3 sees the precursor after it has crossed an open 0.002-inch crack and traveled 5 mm. The stress records obtained from the three gages are shown in Fig. 10.

Each transducer measurement was recorded differentially, as suggested by Petersen, Grine, and Murri,[3] to eliminate external noise (such as piezoelectric signals from the quartz grains) common to the voltage leads. This system produced very satisfactory noise levels as can be seen from Fig. 10; however, all three gages failed about 1/2 μsec after the precursor arrival. The reason for this premature failure is not known definitely, but it probably is caused by shearing of the gage leads either at the

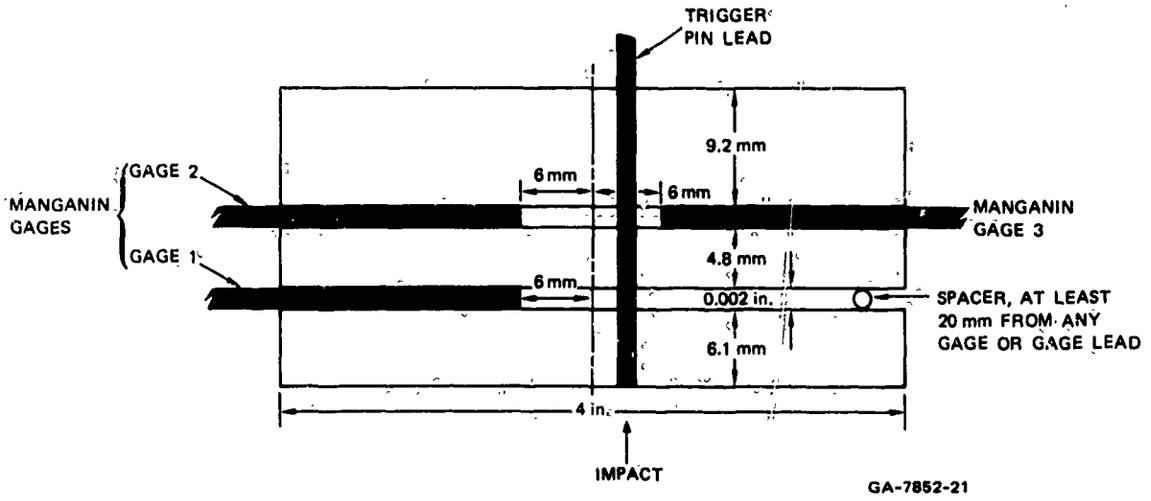

FIGURE 9 SIDE VIEW OF NOVACULITE TARGET, SHOT 982, SHOWING RELATIVE POSITIONS OF GAGES 1, 2, AND 3

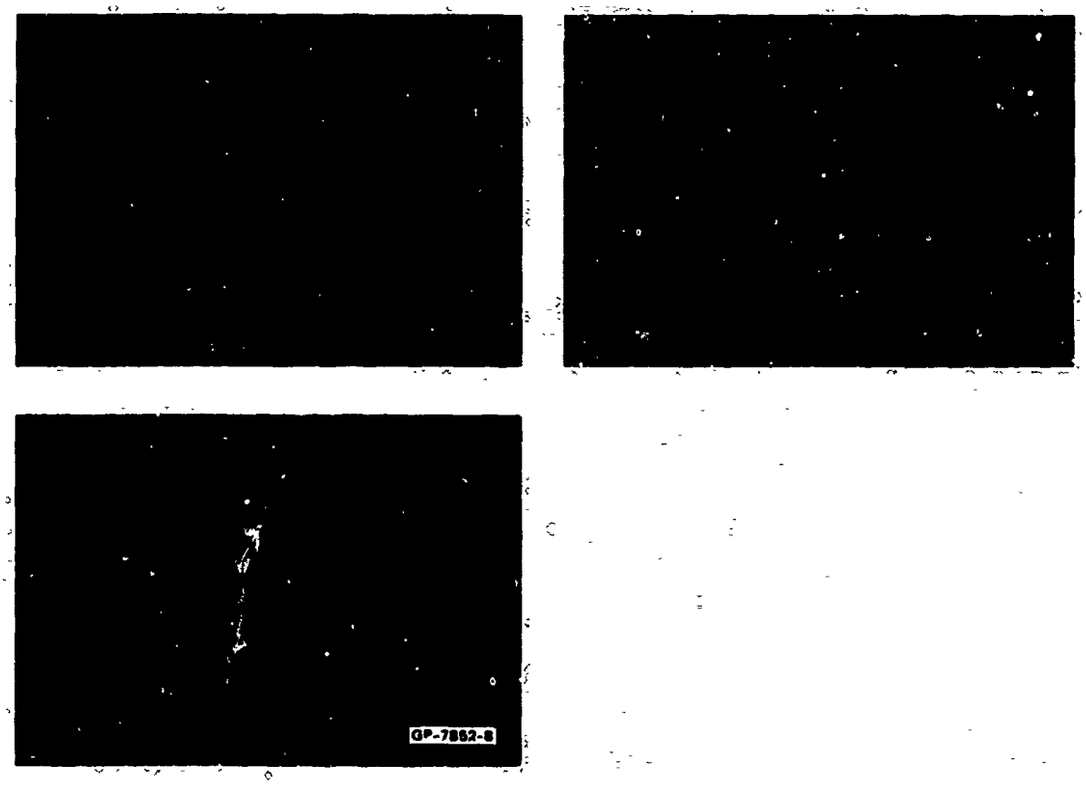

FIGURE 10 MANGANIN GAGE RECORDS FROM GAGES 1, 2, AND 3, SHOT 982; THE RELATIVE LOCATIONS OF GAGES ARE SHOWN IN FIGURE 9. All scopes are sweeping at 0.5 mm/μsec. See text for discussion of stress profiles.

lateral boundaries, or within the target disk. This shearing occurred even though the normal precautions were taken to prevent it: the target was oversize with respect to the projectile, and the leads were mechanically shielded where they left the target. In all subsequent shots, this problem was avoided by bringing the leads out the back of the target through drill holes.

Analysis of the records from Shot 982 yields the following elastic precursor data. Rise times monitored by all three gages are 40-50 nsec. Gages 1 and 2 indicate that stress amplitude at the leading edge of the precursor is about 40 kbar with an increase to 50 kbar by the time the record terminates. Gage 3, above the open 0.002-inch crack, sees an initial amplitude of 60 kbar decreasing to about 50 kbar at the end of the signal. The peak stress is not recorded due to failure of the gages prior to arrival of the main wave; however, for the recorded projectile velocity of 0.97 mm/μsec, the value computed by impedance match is about 100 kbar as in Shot 970.

In reducing the raw gage data to stress profiles, we considered the effect of stress-induced changes in lead resistances and found a 4% correction was required. It also should be pointed out that the manganin piezoresistive coefficient used to analyze Shots 970 and 982 is a value (given in Section V) which has been measured for gage elements embedded in materials shocked above their HEL.[21] There is some indication from low stress gage work now in progress[24] that manganin in elastic materials has a coefficient as much as 30% lower than this. This coefficient is normally checked by comparing peak gage stress with an impedance match solution; however, this is not possible in shot 982 because of the premature gage failure. Consequently, although it is valid to compare gage records in this shot, the calculated precursor amplitudes may be significantly low. This qualification does not apply to Shot 970 since in that experiment the gage element is embedded in C-7, for which a reliable calibration is available.

The similarities of stress profile and amplitude recorded by gages 1 and 2 in Shot 982 indicate that the presence of a 0.002-inch manganin foil gage has a negligible effect on subsequent wave propagation. In particular, presence of the gage does not initiate local rock yielding which can be resolved at later gage stations. The significantly greater HEL observed at gage 3 is attributed to specimen variation since we do not see how it can be an inherent result of propagation across an open crack. Alternatively, the behavior recorded by gage 3 may result from a stress relaxation effect due to the open crack or from a time-dependent yield process in novaculite. No additional experiments were performed on novaculite to resolve these questions in order to conserve time and funds to investigate the dynamic fracture of Westerly granite.

B. Westerly Granite

The elastic precursor amplitude of Westerly granite was measured as a function of distance from the impact surface to a maximum of ~35 mm for dry, dry microfractured, and water-saturated Westerly granite, and for dry Westerly granite loaded at a reduced rate. From these experiments the sensitivity of the dynamic shear strength, or more directly the HEL, to variations in the initial microcrack density, the moisture content, and the strain rate was determined. The initial portions of the release paths were also measured in two of these experiments. Samples of shocked granite were recovered from two experiments for examination. Following a description of the samples, the results of the instrumented and the recovery experiments are presented under (2) and (3).

1. Specimen Description

The Westerly granite specimens studied in the present work were obtained from the Bradford quarries located about 5 miles east of Westerly, Rhode Island. A comparison of the compositions of granites from Westerly and Bradford by Chayes[25] reveals that both are fine-grained granites of similar appearance, but that Bradford specimens are generally about 5% poorer in quartz and 8% richer in plagioclase. He also noted that the biotite flakes in Bradford granite are broader by several tenths of a millimeter and comprise a larger percent of the total than those in Westerly granite. A detailed quantitative description of a sample of Westerly granite

examined in a cooperative effort by 34 laboratories is given by Fairbairn et al.,[26] and a description of a Westerly granite studied in several static and dynamic investigations at General Motors is presented by Green and Perkins[12] and again by Jones and Froula.[13]

The granite studied in the present work has an average density of 2.65 g/cm^3 and a porosity of about 0.015 by volume, calculated from the ability of the rock to absorb water. Petrographic analysis of six thin sections indicates the average composition is about 25% quartz, 40% plagioclase, 30% potash feldspar, less than 5% biotite (mica), and about 1% accessory minerals. The average grain size of the three primary constituents is under 1 mm with a maximum diameter of about 2.5 mm. From thin sections taken in three orthogonal directions, a slight trend toward a biotite orientation was noted, but so many grains had orientations contradictory to the trend of lineation that it is not considered significant and the rock can be called isotropic.

We measured the zero-pressure, longitudinal sound velocity of our specimens to be about 4.2 mm/μsec with a 10% variation from specimen to specimen. These values agree in both magnitude and reproducibility with the results of Simmons and Brace[27] and of Birch.[28] The sound velocity data, taken at 5 locations on each specimen, along with X-ray examinations for internal cracks, were used to select like specimens for each experiment.

We also compared our granite with a Westerly granite studied in triaxial failure tests by Brown and Swanson.[9] (This is apparently the same granite stock studied in the General Motors work.[12,13]) The reported density of this material is 2.619 g/cc with a porosity of 0.007 by volume. Our petrographic analysis shows the quartz content and total feldspar content to be about the same as in our stock; however, the ratio of potash to plagioclase feldspar is inverted, and less of the potash feldspar is microcline. The grain sizes of the major constituents are fractionally less in their material. For the purposes of this report, all the granites discussed above, including our material, will be referred to as Westerly granite.

In summary, the materials characterized in the literature as Westerly granite are obviously similar. Measurable and reproducible differences in composition do exist, and although not unusual in geologic materials, they should be borne in mind when comparing different investigators' measurements of structure-and defect-sensitive properties, such as shear strength.

2. Lagrangian Gage Experiments

a. Westerly Granite, Dry.

In Experiment 7852-0-1 we determined the HEL and the compression and partial release paths for dry Westerly granite shocked to a peak stress of about 60 kbar using the SRI 4-inch light gas gun. These results were calculated using the Lagrangian stress gage analysis[17,16] discussed in Section III. The analysis was performed using a computer program described by Murri and Smith.[4]

Three in-material manganin stress transducers were placed between four 3-inch diameter granite disks in the configuration shown in Fig. 3. The face of each disk was ground flat and parallel to within ± 0.0005 inch. In addition to the bulk density measurements normally made on each disk, each was X-rayed and had the longitudinal sound velocity measured at 5 positions. The sound velocity measurements are reproducible to ± 1% although the absolute accuracy is no better than 5%. They typically show a variation within a single specimen of 5% and variation from specimen to specimen as high as 10%. The four mating disks selected for each experiment did not have observable open internal cracks and usually had less than 5% variation in sound velocity.

The three gages were located along the axis of the cylindrical target at about 1/2, 1, and 1-1/4 inches from the impact plane (front face of the cylinder). To ensure full recording time and accuracy, the leads for each gage were brought out the back of the target through drill holes packed with amalgam. This lead configuration was used in lieu of bringing the leads out the side, which, although simpler to construct, was found to result in premature gage failure in the novaculite shot reported previously. The first two gages were cut from 0.001-inch thick manganin

foil and had an aspect ratio of about 100. For comparison of gage piezoresistive coefficient and noise pickup, the third gage (farthest from impact) was 0.003-inch diameter manganin wire flattened to an aspect ratio of about 10. Differential amplification of gage records as described earlier (see Arkansas novaculite) was used to reduce noise pickup.

The target assembly was impacted by a 4-inch diameter steel-headed projectile traveling at 0.625 mm/μsec. This projectile was a knockout head type designed to allow recovery of shocked granite. The results of the recovery aspect of the experiment are discussed in Part C of this section.

The differential amplification of the gage signals in conjunction with the gage and lead geometry produced records with very low noise. Slightly less noise was recorded from the wire than from the foil gages, as would be expected because of the relative aspect ratios and thicknesses. All three gages lasted longer than the duration of the stress pulse.

The σ_x-t (axial stress-time) histories from the three gage records are plotted on a common time axis in Fig. 11. The calculated records are arbitrarily terminated at or shortly after the arrival of the lateral rarefactions. The stress-time profile from the first gage is essentially linear from less than 5 to about 30 kbar. The rise time is about 10 nsec/kbar, or less than 0.3 μsec for the precursor, and increases at higher stresses. The second and third gage records show similar behavior and differ from the first primarily in that the precursor is farther ahead of the peak and that the trailing rarefaction catches up to and overtakes the peak (gage 3), causing attenuation.

From these records the HEL of Westerly granite is between 27 and 37 kbar. Since 27 kbar is the onset of deviation from linearity in all records, it will be taken as the HEL. Above 40 kbar, the third gage record shows that the compressional pulse is beginning to steepen. Thus the stress-strain curve, the slope of which is related to the compressional wave velocity, is concave upward above 40 kbar; from this we conclude that 40 kbar is clearly above the HEL, although a time-dependent yield process may still be occurring at this stress.

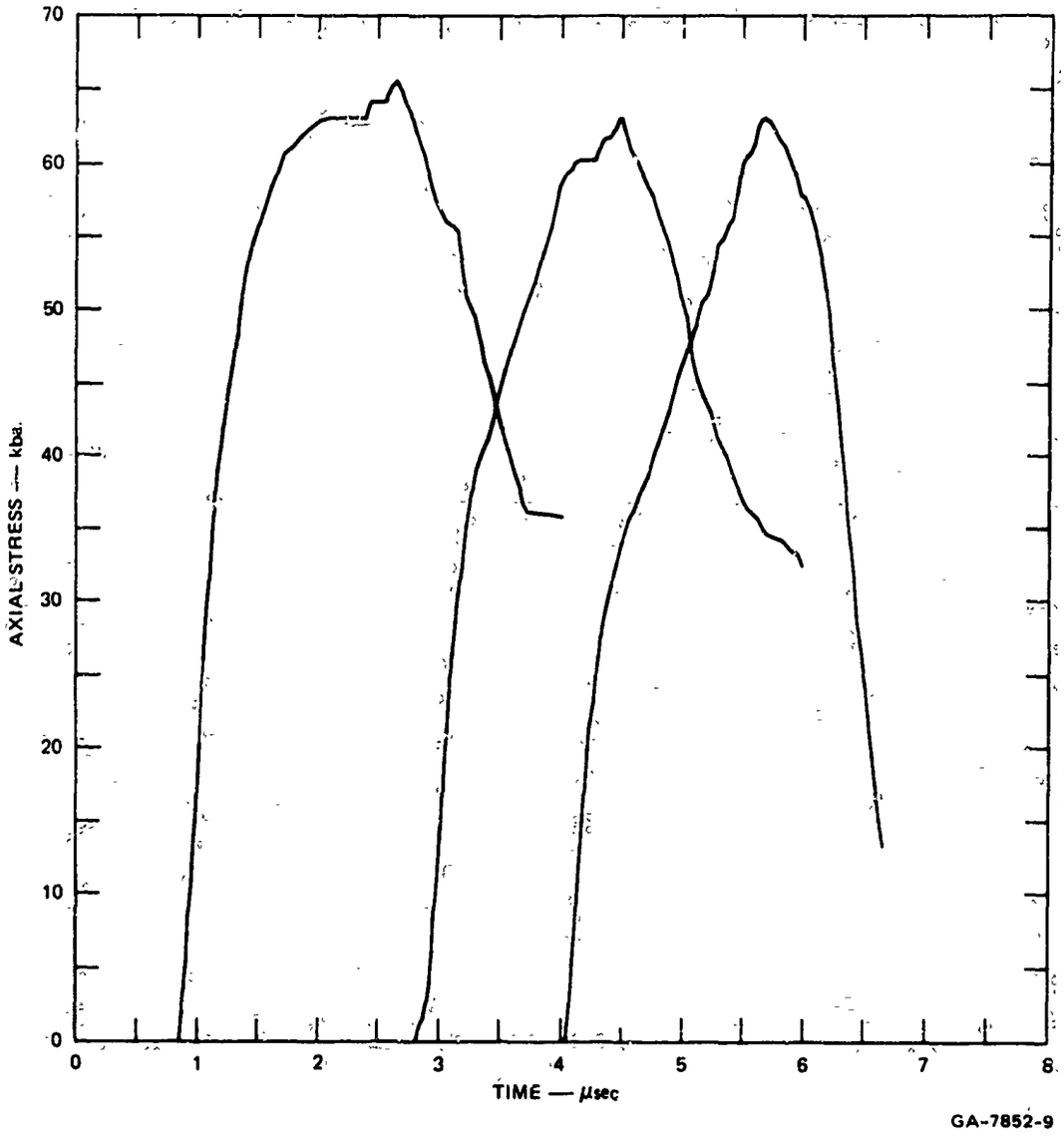

FIGURE 11 AXIAL STRESS-TIME PROFILES AT THREE SUCCESSIVE IN-MATERIAL GAGES, SHOT 7852-0-1, DRY WESTERLY GRANITE. Gages are 11, 23, and 29 mm from the impact surface.

The axial stress-specific volume (σ_x-V) loading curve for some mass element between the first and third gages, calculated using a computer to perform the Lagrangian analysis, is shown in Fig. 12. This is a material average since the three-gage analysis shows C_σ is a slowly varying function of position, being relatively independent of position below 20 and above 50 kbar with the major variation in the yielding range, from 30 to 40 kbar. This variation indicates the yield process either may have a different stress dependence in the two gage intervals (caused possibly by specimen variations) or may still be changing with time and propagation distance.

Below 25 kbar, the σ_x-V relation is nearly linear and is identified as the elastic portion of the Hugoniot. At about 27 kbar, deviation from linearity becomes apparent, hence this stress is confirmed to represent the HEL. From the slope of the elastic portion of the σ_x-V loading curve, we calculate the longitudinal sound velocity to be 5.59 mm/μsec in very close agreement with the value of 5.60 reported by Jones and Froula.[13] This agreement supports the identification of the first linear portion of the loading curve with the elastic Hugoniot. The initial unloading path in Fig. 12 has nearly the same slope as the elastic Hugoniot indicating that the granite is first releasing elastically, like an ideal elastic-plastic material. To confirm this hypothesis we would need to show that the unloading path in fact lies below the Hugoniot in σ_x-V space. Although the Hugoniot curve has not been accurately measured in this stress range, it is extremely unlikely that it is sufficiently curved so that the tangent to it at 60 kbar (which is also tangent to the release isentrope intersecting the Hugoniot at 60 kbar) could have as large a negative slope as does the unloading path we observed. Release data to lower pressures would be required to determine whether there is an elastic-plastic transition in release corresponding to the HEL in compression.

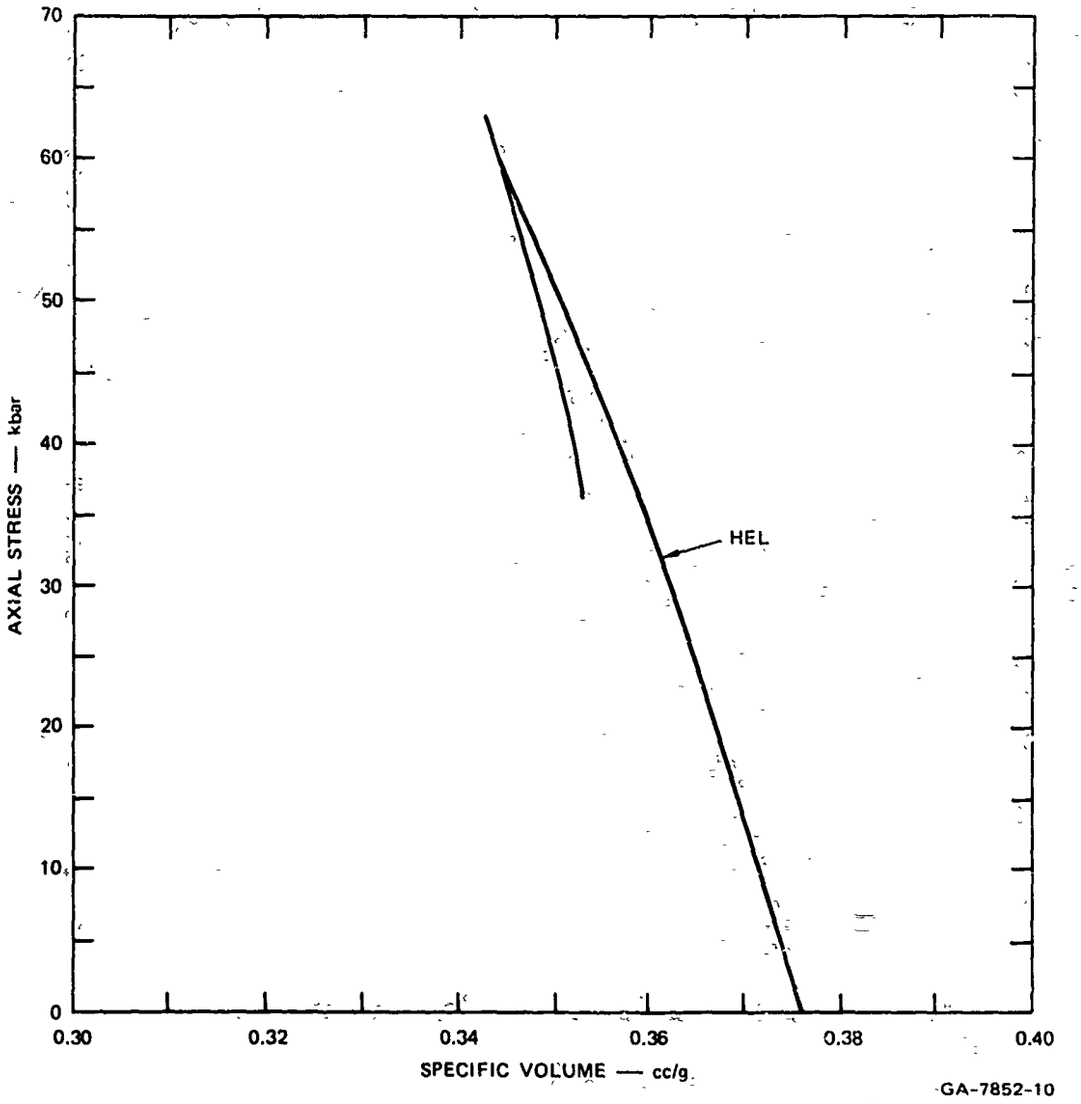

FIGURE 12 AXIAL STRESS-SPECIFIC VOLUME LOADING AND RELEASE PATHS FOR DRY WESTERLY GRANITE. The deviation from linearity in the loading path is taken as the HEL (~28 kbar). The decrease in slope at the end of the release path is due to arrival of lateral rarefactions at the gages and is not significant.

b. Westerly Granite, Dry, Microfractured

It has been demonstrated by Brace et al.,[29] and by Brown and Swanson[9] that Westerly granite, and many other geologic materials, when statically and uniaxially stressed to about 1/2 the ultimate fracture strength exhibit a volume dilatation. That is, above the dilatancy threshold stress, the observed granite volume strain is less than the expected elastic volume strain (which increases linearly with increasing load). The effect is described in detail in references 29 and 9 for various applied triaxial stress configurations. Brace et al. did compressibility experiments to demonstrate that the increase in volume compared to the elastic volume strain was due to open microcracks oriented predominantly in the direction of axial compression, and they suggested several mechanisms whereby such cracks could grow at favorably oriented grain boundaries. Peng and Johnson[30] have performed a detailed petrographic study in which they actually observe the microcracks postulated by Brace et al. and record the number, orientation, and length of these cracks as a function of increasing axial stress. In the present work we wanted to determine the effect of an increased microcrack density on dynamic strength. Consequently we microfractured samples of Westerly granite prior to shock tests, as described below.

The faces of cylindrical 3-inch diameter granite disks of the thickness required for Lagrangian gage experiments were ground flat and parallel within ±0.0005 inch. Circumferential strain gages about 1 inch long were attached using standard strain-gage bonding methods. The instrumented disks were stacked between steel platens to which 3-inch diameter Westerly granite loading cylinders were attached with epoxy. The purpose of these loading cylinders was to prevent platen-sample interactions, such as end splitting, in the specimen disks. The total granite column had a length-to-diameter ratio of at least 2.5 to 1. Mogi demonstrated that with this aspect ratio end effects in granite are insignificant.[31] The specimens were loaded in uniaxial compression to about 1.8 kbar, about 80% of the fracture strength, using a 300,000-lb press. The period for the compression and release cycle was about 30 minutes. Both the strain gage measurements and

and subsequent measurements of bulk density indicate the residual decrease in density for the specimens microfractured in this way to be about 0.1%, the same order of magnitude reported by Brace et al.

The microfractured specimens were used to construct a Lagrangian gage target assembly essentially identical to the granite shot, 7852-0-1, described previously. The same sample selection and gage construction techniques were used. This target was impacted by a 4-inch diameter steel-head projectile traveling at 0.60 mm/μsec. The three stress gage records obtained for this shot are shown in Fig. 13. Analysis of the records was terminated about 6 μsec after impact when an extraneous electrical pulse of unknown origin was recorded by all three gages. For gages 1 and 2 , this event occurs after the release process has been underway for some time, however for gage 3 it happens just as the rarefaction arrives.

The σ_x-V path calculated by Lagrangian analysis is shown in Fig. 14. The loading path was calculated using all three gage records and the full Lagrangian analysis, whereas the unloading path was calculated using only gages 1 and 2 because of the noise in the record from gage 3. The two-gage Lagrangian analysis includes the assumption that C_σ is not a function of position. Based on the results of Shot 7852-0-1, this assumption is probably quite good since the elastic portions of the flow in that experiment were shown to satisfy it.

The σ_x-t records and the calculated σ_x-V path for this shot are nearly identical to those from the dry unfractured specimens. The HEL as indicated both by the stress-strain path and the wave profile is again 27 kbar and the sound velocity calculated from the slope of the elastic portion of σ_x-V path is again 5.6 mm/μsec. The conclusion is that the additional microcracks do not affect either the dynamic shear strength or the elastic constants to the precision of the present shock wave measurements. The fact that the HEL of dry granite is independent of variations in microcracking over the range of the present experiments is an unexpected and important result.

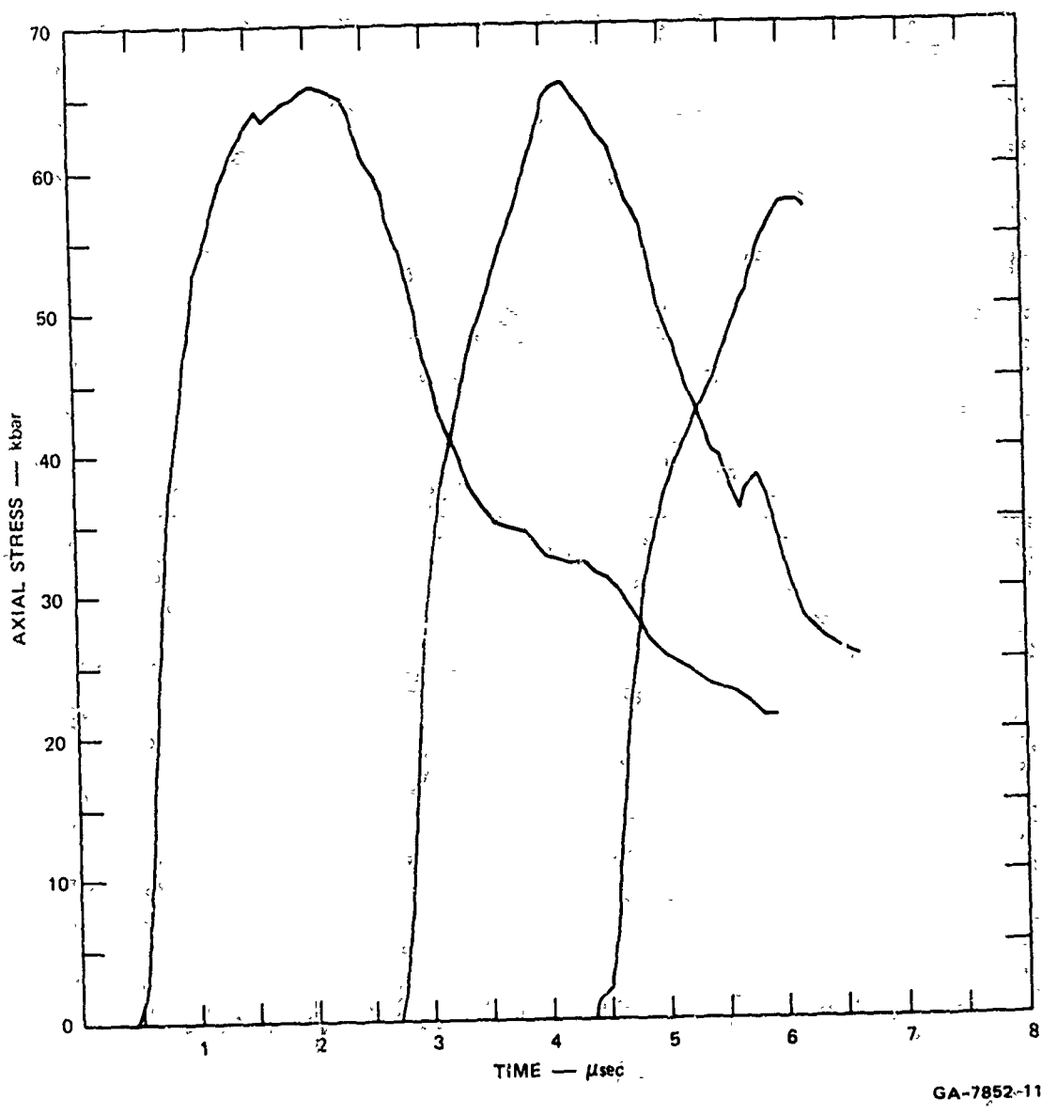

FIGURE 13 AXIAL STRESS-TIME PROFILES AT THREE SUCCESSIVE IN-MATERIAL GAGES, SHOT 7852-0-2, MICROFRACTURED DRY WESTERLY GRANITE. Gages are 12, 25, and 34 mm from impact

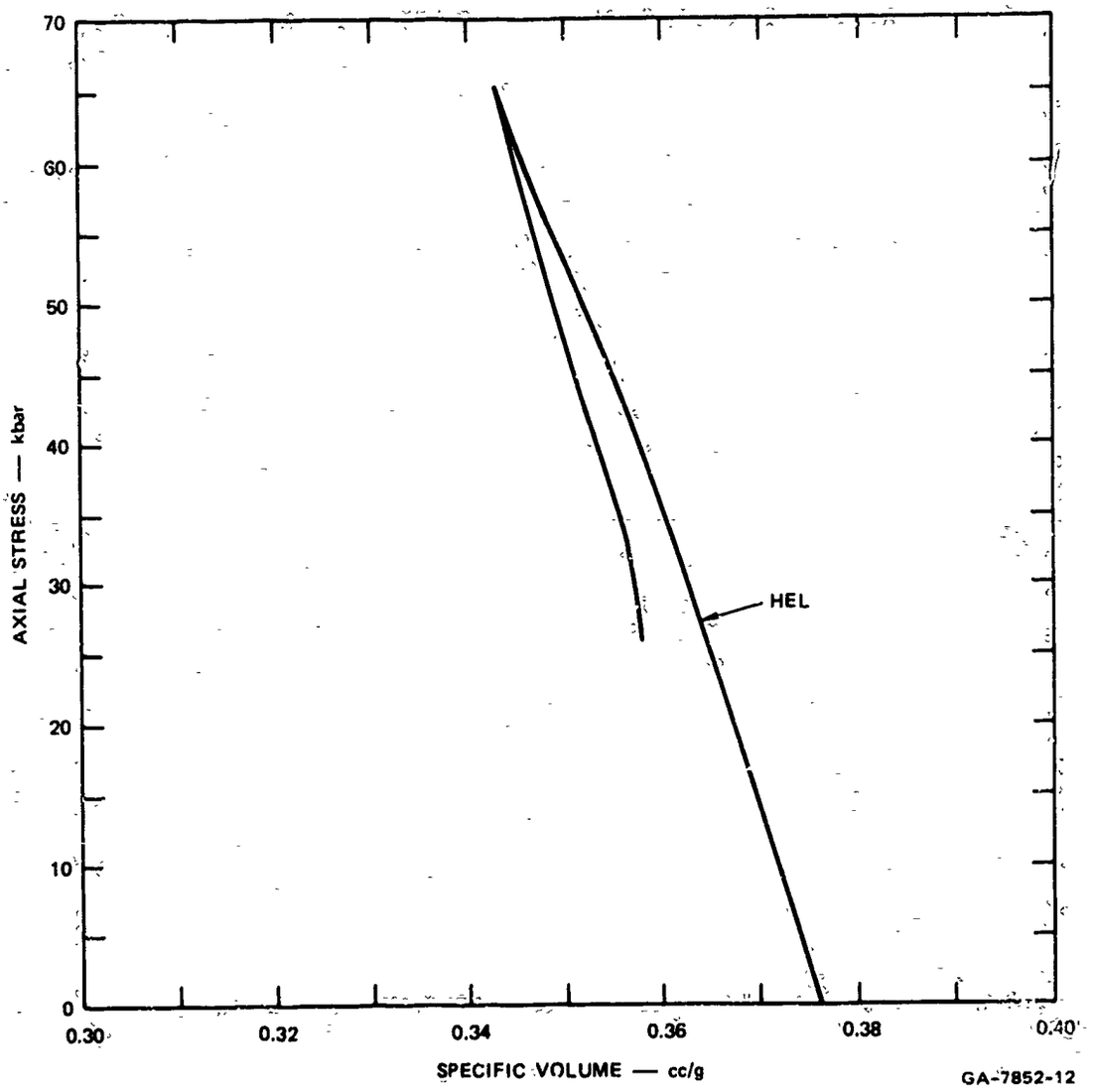

FIGURE 14 AXIAL STRESS-SPECIFIC VOLUME LOADING AND RELEASE PATHS FOR MICROFRACTURED DRY WESTERLY GRANITE. The release path is calculated from gages 1 and 2, Figure 13; the loading path is calculated using all three gages; see the notes in Figure 12.

c. Westerly Granite, Saturated

Samples of Westerly granite were saturated with water in the following manner. The specimens were first baked and outgassed. While under vacuum, they were submerged in degassed heated water and then raised to atmospheric pressure. At this stage in the saturation process 1 atm pressure drives water of reduced viscosity (because of the heating) into the evacuated pores. To accelerate the absorption process and to ensure that the rocks become completely saturated, we imposed a 100-psi external pressure. Our data indicate that the additional overpressure is required to totally saturate this rather impermeable rock. The rock porosity filled with water by this procedure was about 1.5% by volume and is assumed to represent 100% saturation.

A three-stress-gage Lagrangian target assembly of the same configuration used in Shots 7852-0-1 and 7852-0-2 was assembled using the saturated disks. The saturated granite target was mounted on a high lead brass driver plate and surrounded by a water-and vacuum-tight cell of slightly larger internal volume than the target. This volume was filled with water to ensure that the granite did not lose moisture during the firing sequence. The assembly supported the 100-μ vacuum to which the muzzle of the gun is pumped prior to shooting.

All three gages were cut from 0.0007 inch manganin foil and were the same configuration used for gages 1 and 2 in Shots 7852-0-1 and 7852-0-2. They were electrically insulated from the saturated rock by a thin layer of C-7 epoxy on each face of the laminate disks. The total thickness of each gage layer was about 0.0015 inch. The leads were brought out the back of the target through insulated holes.

The 0.2-inch thick high lead brass driver plate on which the granite target was mounted was impacted by a 4-inch gas gun projectile with a high lead brass head. Projectile velocity was 0.51 μsec/cm and the peak stress in the granite was about 50 kbar. The first gage was about 1/4 inch into the granite from the granite-driver interface, and each gage was separated by 1/4 inch of granite, so that the measurements were made between 1/4 and 3/4 inch from impact. The last granite disk was 1/2 inch thick to keep any

signals from the rear surface from arriving back at the gage positions during the measurement period. Instrumentation was by the differential amplification scheme to reduce external noise pickup.

The σ_x-t stress profiles are shown in Fig. 15. Compared to the records for dry granite and dry microfractured granite these are quite linear and do not show the type of two-wave structure that developed rather clearly in the third gage record in the previous two experiments. The maximum gage distance from impact was 3/4 inch in this experiment and about 1-1/4 inches in the previous experiments. Rarefaction data were not obtained in this experiment because the projectile head was thick for optimum recording of loading data.

The σ_x-V loading path from a 3-gage Lagrangian analysis is presented in Fig. 16. This path is linear within experimental error as opposed to the marked curvature noted in the previous two experiments for dry granite. The slope of the loading path is significantly less than in the previous two experiments. A hypothesis which accounts for all the observed differences between the data for dry and water-saturated granite is that the dynamic shear strength of saturated granite is markedly less (at least an order of magnitude less) than that of the dry granite. Evidence to support the conclusion that the shear strength of wet granite is essentially zero is presented in Section V.

d. Westerly Granite, Dry, Reduced Loading Rate

Barker and Hollenbach[22] have recently confirmed Wackerle's observation[32] that, below 40 kbar, fused quartz is dispersive to shock loading; that is, it has the unusual property of causing a steep shock front to spread with propagation distance. This behavior results from anomalous curvature of the fused quartz elastic Hugoniot below 40 kbar. Because of this property, a thick fused quartz plate mounted in front of a target specimen in a shock experiment can be used to reduce the loading rate in the target compared to direct impact. The technique will work only if the maximum stress in fused quartz is less than 40 kbar. Since the HEL measured for dry Westerly granite is below 40 kbar and granite has a slightly higher shock impedance than fused quartz, we can use the

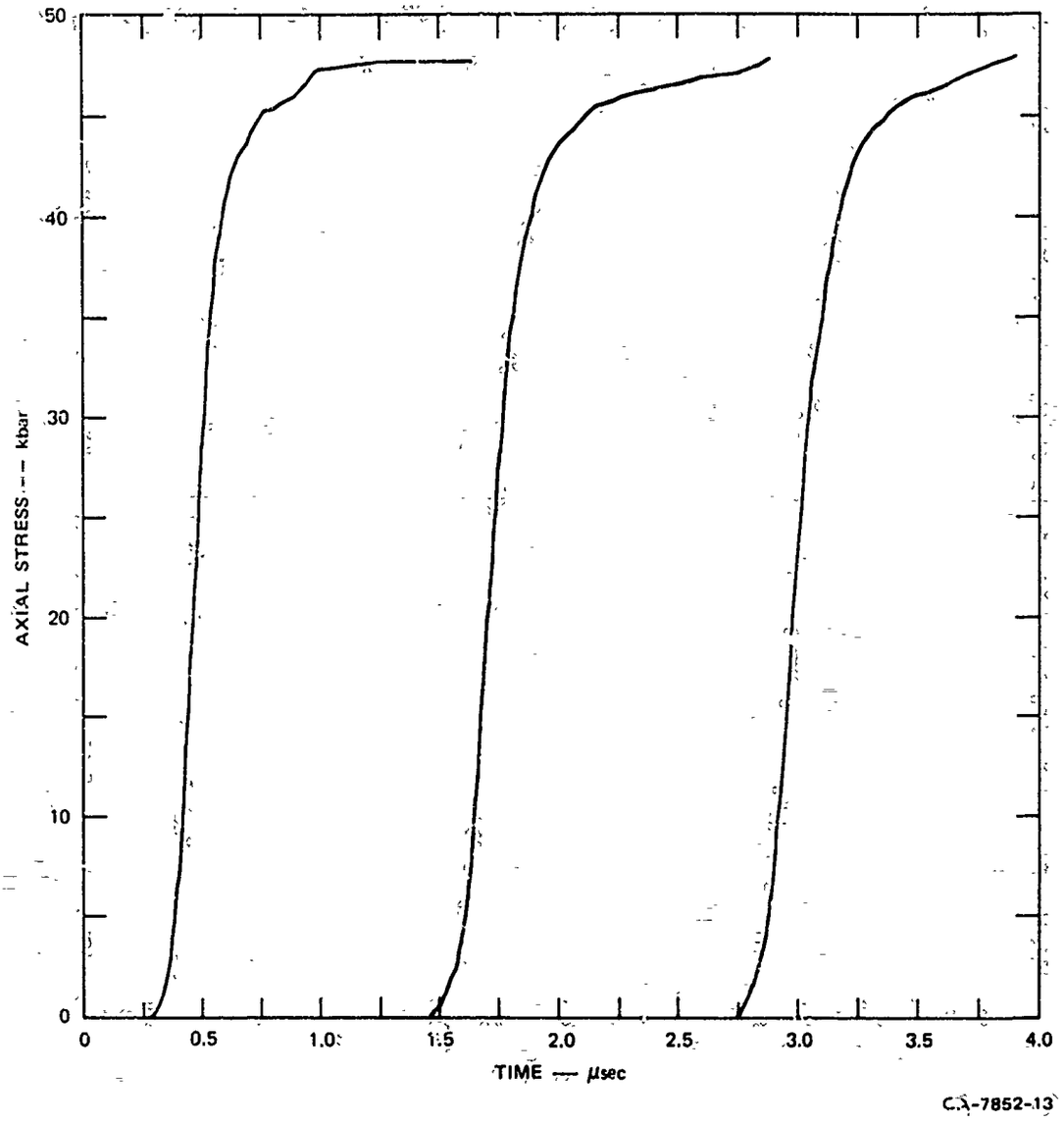

FIGURE 15. AXIAL STRESS-TIME PROFILES AT THREE SUCCESSIVE IN-MATERIAL GAGES, SHOT 1035, SATURATED WESTERLY GRANITE. Gages are 7, 13, and 20 mm from the driver plate.

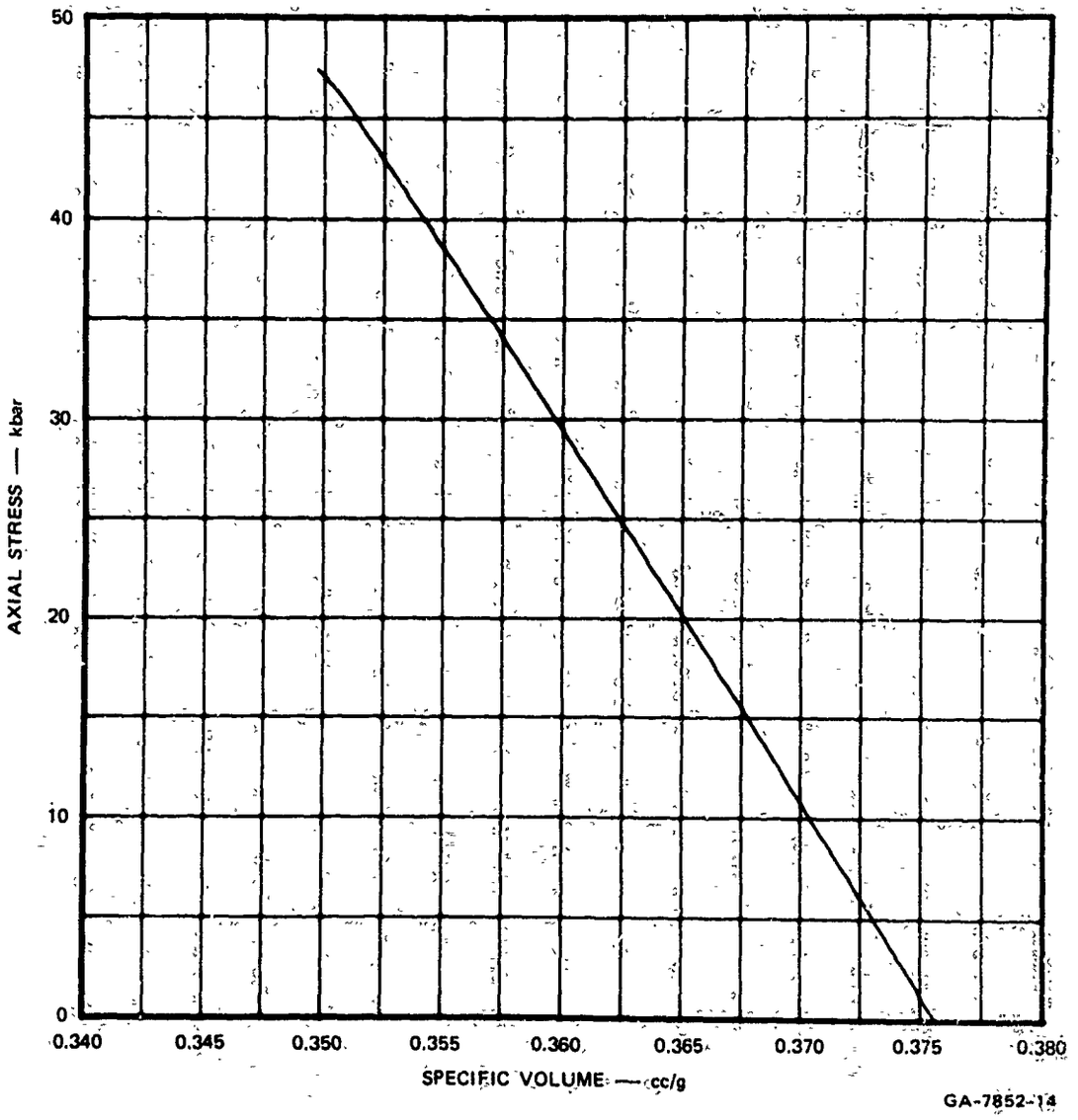

FIGURE 16 AXIAL STRESS-SPECIFIC VOLUME LOADING PATH FOR SATURATED WESTERLY GRANITE, SHOT 1035

method to obtain reduced rates of loading in granite and still exceed the HEL. We performed such an experiment to observe the dependence of dynamic shear strength on loading rate.

A one-inch thick, 4-inch diameter disk of G. E. Type 151 fused quartz was epoxied to Westerly granite target assembly. This target assembly consisted of three in-material manganin foil gages separated from the fused quartz and each other by 1/4-inch thick, 3-inch diameter granite disks, and backed with 1/2 inch of granite. The details of target design and construction are the same as for the previous granite shots. The fused quartz was impacted by a standard 6061-T6 4-inch gas gun projectile traveling at 0.53 mm/μsec.

The three σ_x-t records are shown in Fig. 17. The rise time from 0 to 30 kbar at gage 1 is about 0.8 μsec, or a decrease of about a factor of 3 compared to gage 1, Shot 7852-0-1. The profile steepens and becomes more linear as it passes gages 2 and 3. The 0- to 30-kbar rise time at gage 3 is about 0.55 μsec. Above about 30 kbar the slope of the σ_x-t profile begins to decrease and the stress continues to rise until the records terminate. No distinct second wave is seen. These records are consistent with an HEL of about 30 kbar, but the propagation distance is not long enough and the final stress not high enough to determine if a two-wave structure is definitely developing. Unfortunately these parameters are limited by the diameter of the gun and equation of state of fused quartz, respectively.

The σ_x-V loading path is given in Fig. 18. It is linear to just over 30 kbar. If this linear section is identified with the elastic Hugoniot, the sound velocity calculated from the slope is 5.53 mm/μsec or about 1% less than the value measured in Shots 7852-0-1, 7852-0-2, and by Jones and Froula.[13] This agreement supports the Hugoniot interpretation. The major conclusion from this experiment is that the HEL is not sensitive to small changes in loading rate.

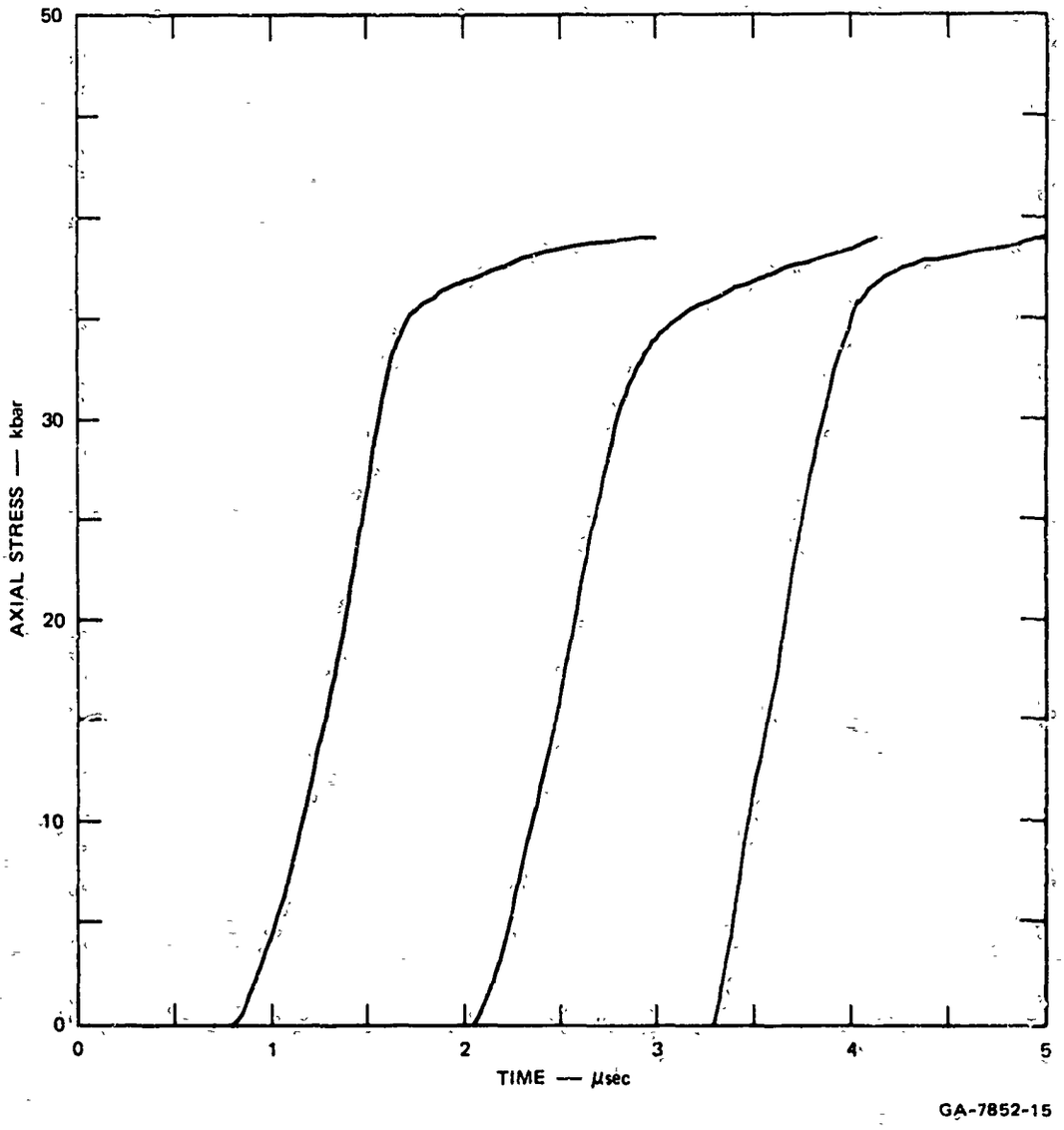

FIGURE 17 AXIAL STRESS-TIME PROFILES AT THREE SUCCESSIVE IN-MATERIAL GAGES, SHOT 1033, DRY WESTERLY GRANITE LOADED AT A REDUCED RATE. Gages are 6, 13, and 19 mm from the fused quartz.

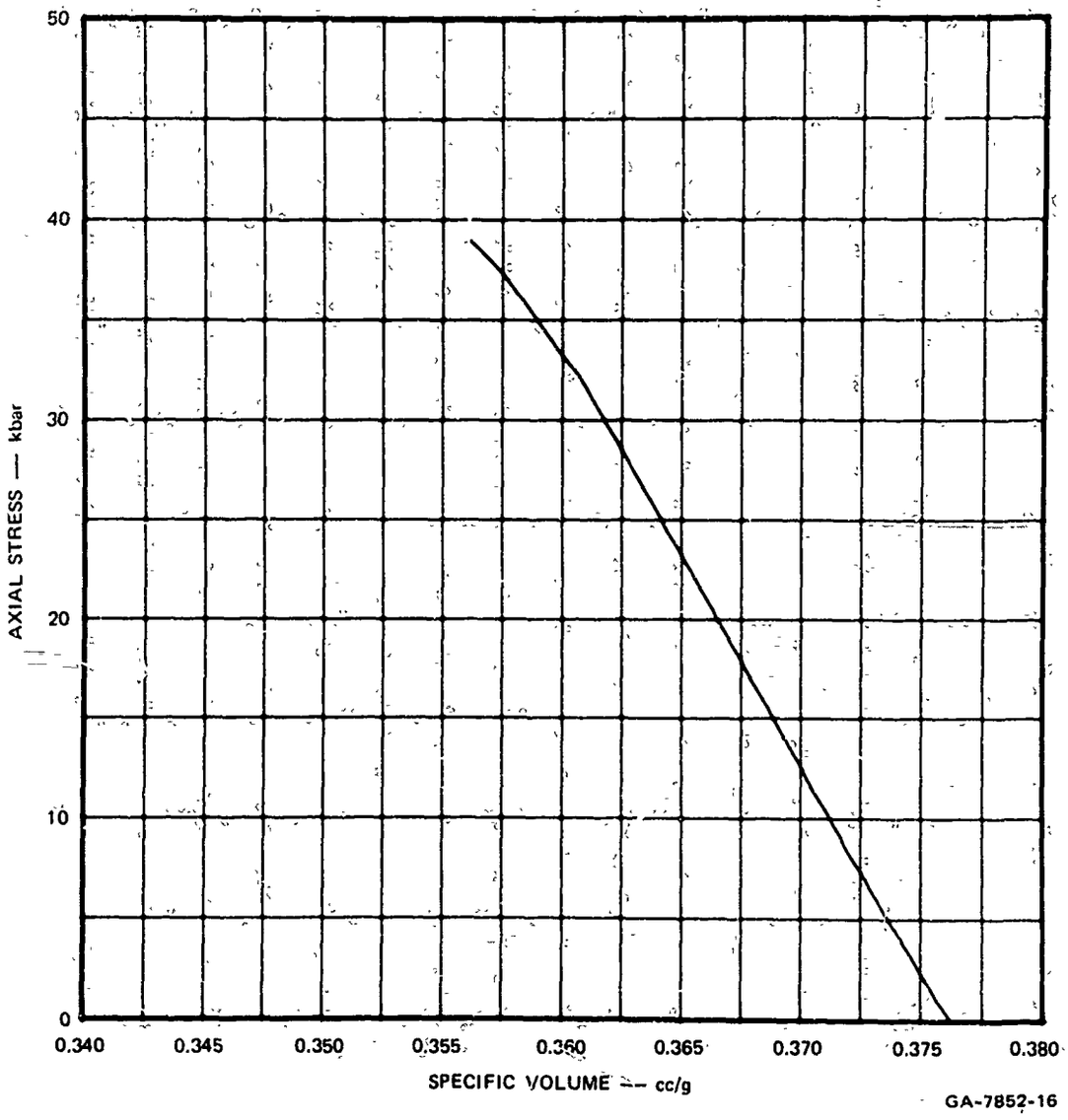

FIGURE 18 AXIAL STRESS-SPECIFIC VOLUME LOADING PATH FOR DRY WESTERLY GRANITE LOADED AT A REDUCED RATE, SHOT 1033

3. Recovery Experiments

Two experiments were performed in which Westerly granite shocked above its HEL was recovered. The first of these was Shot 7852-0-1, the instrumented dry Westerly granite shot described previously in which the peak stress was about 60 kbar. In this experiment the inside diameter of the projectile body was larger than the outside diameter of the granite target. The steel head of the projectile was designed to allow it to be knocked out through the projectile body upon impact with the granite target. The projectile body then passed over the granite target; and the granite, the projectile body, and knockout head were all caught in a small tank. This tank is free to move in the direction of projectile motion within a large evacuated catcher tank at the end of the muzzle and is gradually stopped by rags loosely stuffed in the large tank.

The recovery system worked as designed and about 90 g of granite of the original 430 g were separated from the shot debris. The recovered material was a fine dust; 90 mass percent of the material, as determined by sieving, was between 40 and 600 μ in size. The average grain size of the virgin material was found by petrographic examination to be just under one mm (1000 μ). The 90 g of recovered material was found to obey a log normal distribution by mass; that is, the log of the mass percent of material passing through a given mesh versus the log of the mesh size is a linear relation. Such a distribution is usually indicative of a random pulverizing of a brittle material. However, this result must be considered quite tentative since only about 1/4 of the material was recovered. Only if the recovered 90 g was a perfectly random sampling of the fractured rock (which it probably isn't since dust smaller than 40μ is probably not recovered) would the log normal distribution be characteristic of the shock fracture process.

This experiment has two major limitations. The first is that the target assembly had no surrounding momentum traps and hence experienced rarefactions originating at all free boundaries. Consequently, the strain experienced by some of the sample was not uniaxial and the stress history of any recovered piece is not well defined. The second limitation is that

not all of the target can be recovered for later analysis. To remove both these limitations a second recovery experiment was performed. The entire granite disk was shocked beyond the HEL and released to zero axial stress in uniaxial strain, and all the granite was recovered. This experiment was performed using an explosively-driven flyer plate rather than the gas gun to load the sample.

In this "clean" recovery experiment, we kept the flow uniaxial throughout the granite specimen by encapsulating it in almost fully dense pressed NaBr. Since the shock impedance of NaBr closely matches that of granite, the rarefactions that would otherwise originate at the lateral boundaries of the granite and alter the uniaxial nature of the flow do not form. The rarefactions which do originate at the lateral boundaries of the NaBr do not reach the granite until after stress has been released from the back of the flyer plate.

The granite specimen was a disk of about 1-inch diameter and 1/4-inch thickness. This specimen was nominally dry, but in contrast to the gas gun experiments in which the dry specimens are exposed to the muzzle vacuum prior to shooting, this specimen was not evacuated and hence contained some moisture picked up from the atmosphere prior to encapsulation. When it was encapsulated in NaBr, the final target dimensions were about 4 inches diameter by 1-1/4 inches thick. The granite disk was positioned concentrically within the NaBr and about 1/8-inch from the impact surface. The encapsulation was accomplished in three separate pressings. From the first pressing, we obtained a disk of about 1-1/2 inches in diameter with a NaBr density greater than 95% of the theoretical value-- 3.2 g/cc--whereas for the final 4-inch NaBr disk, the average density was about 90% of theoretical. Such a density gradient is satisfactory for lateral momentum trapping, while the high NaBr density near the granite ensures a good impedance match. We used an explosive plane wave generator to project a 1/8-inch thick Al flyer plate into the target assembly at about 0.7 mm/μsec, generating a peak stress of about 50 kbar in the granite. The recovery was accomplished by firing the shot into a small tank of water. The water of course greatly simplifies the separation of granite from the soluble NaBr although the orientation of the recovered material with respect to the shock axis is lost.

The size distribution of the recovered granite pieces was again determined by passing them through a set of graduated mesh size sieves. As in the previous recovery shot in which lateral rarefactions were not prevented from propagating in the granite, the recovered pieces followed a log normal distribution by mass. Some 95 mass % of the recovered fragments had diameters between 0.05 and 1 mm, so many pieces were again of subgrain size. However, in contrast to the first recovery experiment, the clean experiment yielded two relatively large pieces, several millimeters in diameter, and not nearly so many particles of less than 50μ in size. Thus, as expected, lateral rarefactions such as in Shot 7852-0-1 seem to produce a higher density of intragranular fractures and more dust-sized particles than does a single uniaxial strain rarefaction alone.

The two largest recovered pieces are shown in Fig. 19. A single thin section was prepared from the larger recovered piece. A photomicrograph of a part of it and of a nonshocked piece for comparison are shown in Fig. 20. Grains in the shocked piece are traversed by an irregular mosaic of microfractures, some of which cross grain boundaries. By comparison grains in the virgin material look nearly perfect. In addition to the microfracture damage common to all three of the major constituents, some feldspar grains show granulation. That is, within a given grain, subgrains have formed and rotated with respect to the original orientation; this type of damage is common to feldspars shocked to moderate stresses. The quartz grains are microfractured but do not show either granulation or planar features. The mica is microfractured and contains kink bands. Sphene grains are also severely damaged but do not show evidence of granulation. The grain boundaries are very tight. These features are all characteristic of granite shocked to moderate stress levels, say 50 to 100 kbar. Petrographic examination to date has not indicated damage features which distinguish this thin section loaded and released in strict uniaxial strain from granites shocked to similar stress levels in other geometries.

An attempt was made to reconstitute a granite sample for HEL measurements from the material recovered in Shot 7852-0-1. The recovered dust was loaded triaxially to over 30 kbar. The sample so obtained showed some integrity but was not deemed strong enough to hold together during shot construction. The attempt to fire a gage shot on recovered material was not pursued further.

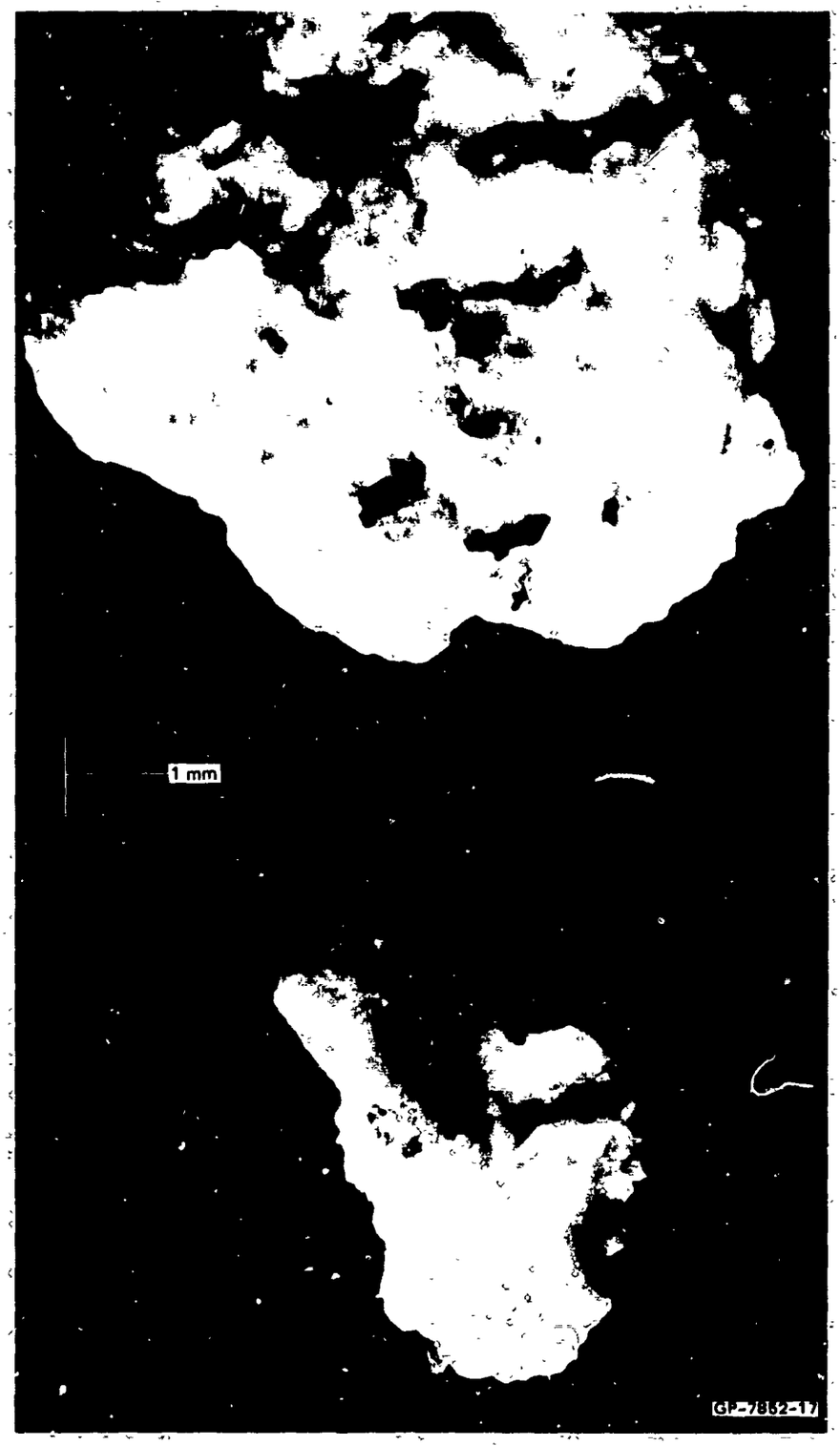

FIGURE 19 TWO OF THE LARGEST PIECES OF WESTERLY GRANITE RECOVERED AFTER SHOCK LOADING TO 50 kbar

FIGURE 20 PHOTOMICROGRAPHS OF THIN SECTIONS OF (a) UNSHOCKED AND (b) SHOCKED AND RECOVERED WESTERLY GRANITE

V DISCUSSION OF RESULTS

From our Arkansas novaculite experiments we observed an HEL of from 40 to 65 kbar for a peak shock stress of about 100 kbar. The best weighted average of these values is 55-60 kbar. This value is near the low end of the range observed in high explosive shock experiments on polycrystalline[19,23] and single crystal quartz.[19,23,32] Since, in this stress range, the precision of the present experiments is significantly greater than that in the earlier high explosive work; we consider 55-60 kbar to be the best current value for the HEL of novaculite shocked to about 100 kbar.

Close agreement is demonstrated in Figs. 5 and 6 between predicted and observed loading profiles for novaculite shocked elastically by a laminated projectile. Two PUFF simulations of this experiment were performed using different assumed elastic equations of state for novaculite. In one it was assumed that the σ_x-V relation was linear (equivalent to linear σ_x-ϵ) and in the other that σ_x-ρ was linear. Published Hugoniot data were not sufficient to distinguish between these two; however, the associated wave propagation properties are quite different. The first relation has the property that a wave front propagates without changing shape, whereas the linear σ_x-ρ relation predicts that a given wave shape will steepen as it propagates. Our experiment agreed much more closely with the profile predicted by PUFF using the linear σ_x-V relation and hence we conclude that this is the best constitutive relation for plane-shocked novaculite below its HEL.

A novaculite HEL experiment, Shot 982, was designed to determine the effect of an in-material gage on local strength. No decrease in strength was observed. This result demonstrates that the HEL is not sensitive to inclusions even with large variations in shock impedance as long as these are sufficiently thin.

We measured the HEL of dry Westerly granite specimens up to 35 mm thick to be about 30 kbar, in contrast to the observation by Jones and Froula[13] on 12.7 mm thick specimens that granite is elastic to over 40 kbar. However, their experimental measurements were made using quartz gages and suffered from severe noise problems above 20 kbar. Our measurements had no such noise problems but they require knowing the piezoresistant

coefficient of manganin. We used the constant value reported by Keough[21] from many measurements between 20 and 290 kbar:

$$P(\text{kbar}) = \frac{\Delta R}{R}\left[(0.29 \pm 0.01) \times 10^{-2}\right]^{-1}$$

Both our work and Jones and Froula's indicate the elastic precursor velocity, as calculated from the slope of the elastic Hugoniot for the loading curve, to be about 5.6 mm/μsec. This agreement indicates good correlation between our respective stress gage calibrations. Because wave profile resolution increases with specimen thickness and with gage signal-to-noise ratio, we feel our observation of a 30-kbar HEL for dry granite is a more reliable determination.

Gregson et al.,[33] on the basis of their own laser interferometer data and a reanalysis of Jones and Froula's data, reported a 17-kbar HEL in Westerly granite and a second anelastic limit or phase transformation at about 40 kbar. We did not resolve a 17-kbar elastic precursor. It is possible, however, that before the dynamic shear yielding at the 30- or 40-kbar HEL, another stress-induced anelastic process occurs. If such a process does occur in the shock front, it does not cause a sufficient change in the elastic moduli to be detected in our Lagrangian gage experiments.

It is interesting to note that in recent static triaxial tests of Westerly granite conducted by Brown and Swanson,[9] it was found that the uniaxial strain loading path never crossed the granite triaxial fracture envelope. In fact, they found the fracture envelope and the uniaxial strain loading path were diverging at the highest stresses they studied. This implies that the granite triaxial shear strength increases faster with mean stress than the stress deviator. However since the maximum axial stress Brown and Swanson reached in uniaxial strain was only 11 kbar, it is possible that their results do not hold at 30 kbar, the HEL we measured for Westerly granite. Brace[11] has extended the static uniaxial strain data for Westerly granite to about 25 kbar without failing the specimen. However, his work does not also extend the fracture envelope, so we do not know whether the triaxial strength of the granite is continuing to diverge from the stress deviator at these stresses, or whether they have begun to converge.

Partial release paths for dry Westerly granite are shown in Figs. 12 and 14. The slope of these paths is quite close to that of the elastic Hugoniot, indicating that granite releases as predicted by simple elastic-plastic theory. This behavior is significant in that it indicates the shear strength of shocked granite is not negligible immediately after shock compression. Note that another estimate of the dynamic shear strength at the Hugoniot state in the present experiments (about 65 kbar) could be obtained from the offset between σ_x measured in our experiments and the hydrostat at the final volume, if we had a good estimate for the hydrostat at this volume. Because of the difference in time scales, our result of a non-negligible shear strength at 60 kbar for a laboratory specimen is not inconsistent with the hypothesis of Godfrey[1] that the shear strength of granite in large scale or nuclear events is probably a fraction of a kbar. The increase in slope at the end of our release data is probably caused by arrival of the lateral rarefaction and is not significant.

One of the important findings of the present work is that the HEL of dry granite is not affected by increasing the microcrack density. The actual microscopic process which limits the dynamic shear stress above the HEL may not involve microcracks at all, or at least microcracks of the orientation induced by the dilatancy procedure we employed. This seems unlikely since microcracks are probably among the areas of least shear strength in the rock. Therefore we conclude that although varying the microcrack density may affect the mechanism of plastic deformation significantly (for example in size of fracture products, or time dependence of fracture) it does not affect the threshold stress for activation, the HEL. Since these microfractures do not lower the HEL, they do not play the shear-stress-relaxing role assigned to block boundaries in Godfrey's rheological model. Thus, microfractures can apparently be neglected in characterizing a material for stress wave calculations.

We also noted no decrease in the HEL when the loading rate was reduced a factor of three compared to direct impact shock loading. The

THIS
PAGE
IS
MISSING
IN
ORIGINAL
DOCUMENT

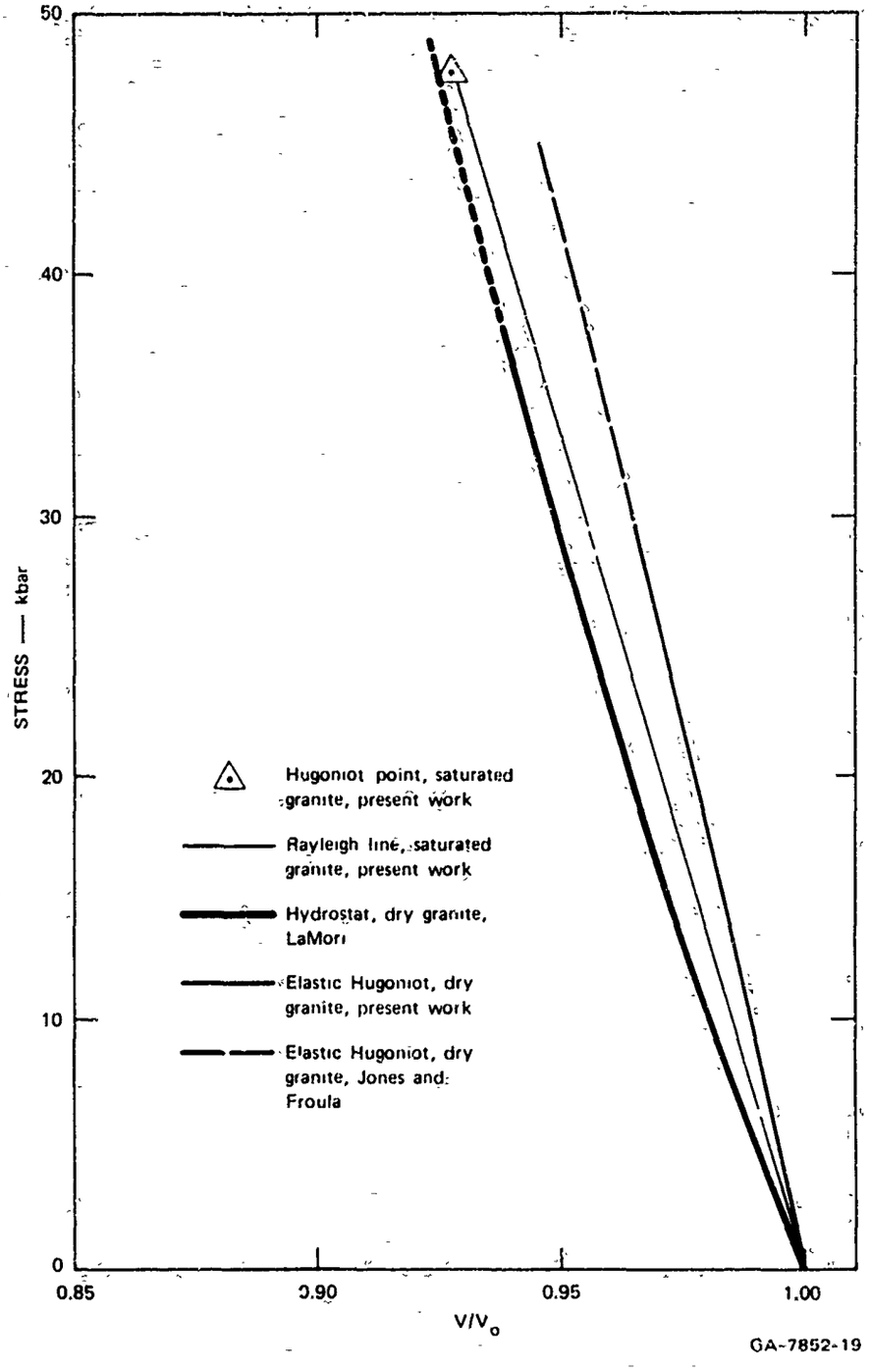

FIGURE 21 HUGONIOT STATE FOR SATURATED WESTERLY GRANITE COMPARED TO THE DRY GRANITE HYDROSTAT AND ELASTIC HUGONIOT. The dashed portion of the hydrostat is an extrapolation of LaMori's data.

The shocked, recovered granite thin section shown in Fig. 20 is unusual in that the loading history was very well defined--planed shocked to 50 kbar for just under 1 μsec and released in uniaxial strain. The recovered material thus has gone through basically the same cycle as the material on which we made our Lagrangian measurements and it was also nominally dry. The pertinent features of the recovered piece are that the grains are still tightly cemented, all the grains are apparently randomly microfractured, and no unusual features that can be related to the uniaxial strain constraint are readily apparent. It is not known whether the observed microfracturing occurs near the HEL or at some other stage in the load-release cycle, possibly the radial flow phase occurring after the axial stress has reached zero (see Fig. 1).

A mechanism for the plastic deformation taking place at the HEL which is consistent with the results of the present investigation is the following. Planes of weakness exist in the dry rock, probably the surfaces of microcracks. There is a threshold shear stress in uniaxial strain needed to activate slip along these planes. This stress is estimated, assuming a Poisson's ratio 0.25 from Brace[11] and an HEL of 30 kbar from the present measurements, to be

$$\frac{\sigma_1 - \sigma_2}{2} = \frac{30-10}{2} = 10 \text{ kb} \quad \text{(mean stress} \cong 17 \text{ kbar and normal stress} = 20 \text{ kbar)}$$

This is slightly less than the 12.5 kbar value calculated from Byerlee's measurements of the coefficient of static friction across ground surfaces of Westerly granite for a normal stress of 20 kbar.[36] Although the disagreement is not large considering the simplifying assumptions made in the calculations and the uncertainty in the value of Poisson's ratio, it is in the wrong direction since there is undoubtedly additional asperity locking across natural surfaces and the difference in loading rates would be expected also to increase the shock value. Thus it is quite possible that other slip mechanisms with somewhat lower threshold stresses are also active in the dry granite at the HEL. There is no reason to expect either a friction-locking process or other slip processes in the dry material to

be sensitive to small changes in rate at these high rates, and we saw no rate dependence. Changing the microcrack density or orientation d ; not affect the threshold stress, so we conclude that the number of slip p'anes in the dry unmicrofractured material is sufficient to nucleate the required plastic flow.

Saturating the specimen with water completely fills the connected microcracks. When the normal stress across the cracks builds rapidly in the shock front, the water has nowhere to go and, because of its lack of compressibility, it holds the crack surfaces apart even at nigh normal stresses. The shear stress supportable by the separated surfaces is essentially the value they can support at zero normal stress. This shear strength may be approximated as the shear strength of the dry rock with no normal force across the crack.

Our model says that filling the microcracks with water introduces planes in the granite which can support only negligible shear and causes the HEL to drop dramatically. The model does not prove, however, that the microcracks are the controlling planes of weakness which determine the HEL in dry rock (although it seems likely). It is possible that plastic deformations also occur in some constituent or constituents, such as shear or kink banding in the mica, and that these are also important in determining the HEL of dry granite.

All of the results discussed in this section suggest that the process occurring at the HEL is not complete fracture of the rock as is usually assumed, but instead is a localized yield and plastic flow which leaves the specimen macroscopically intact.

REFERENCES

1. Godfrey, Charles S., "Calculations and Experiments on the Dynamic Properties of Rocks," Proc. Strategic Structures Research, Long Range Planning Meeting, Vol. 1, 1969 DASA 2288-I.

2. Keough, D. D., C. W. Smith, and M. Cowperthwaite, "Constitutive Relations from In Situ Lagrangian Measurements of Stress and Particle Velocity," Interim Report, Stanford Research Institute, prepared for DASA, Contract DASA 01-70-C-98, 1971.

3. Petersen, C. F., D. R. Grine, and W. J. Murri, "Scaling Problems of Wave Propagation in Rocks," Final Report, Stanford Research Institute, DASA 2579, 1970.

4. Murri, W. J., and C. W. Smith, "Equation of State of Rocks," Interim Technical Report, Stanford Research Institute, for U.S. Atomic Energy Commission, Lawrence Radiation Laboratory, Contract AT(04-3)-115, SRI Project PGU-6618, 1970.

5. Rosenberg, J. T., T. J. Ahrens, and C. F. Petersen, "Dynamic Properties of Rocks," Final Report, Stanford Research Institute, DASA 2112, 1968.

6. Handin, John, "Studies in Rock Fracture," 9th Quarterly Technical Report Texas A & M University, Contract No. DACA 73-68-C-0004, ARPA Order No. 1074 Amendment 1, 1970.

7. Perkins, R. D., A. H. Jones, S. J. Green, and J. D. Leasia, "Determination of Multiaxial Stress Behavior of Solenhofen Limestone and Westerly Granite," Final Report, General Motors Corporation, DASA 2438, 1970.

8. Stephens, D. R., E. M. Lilley, and H. Louis, "Pressure-Volume Equation of Consolidated and Fractured Rocks to 40 kbar, Int. J. Rock Mech. Min. Sci. Vol. 7, pp 257-296, 1970.

9. Brown, W. S., and S. R. Swanson, "Constitutive Relations for Westerly Granite and Cedar City Tonalite for a Variety of Loading Conditions," Final Report, University of Utah, DASA 2473, March 1970.

10. Swanson, S. R., "Dependence of Earth Material Properties on Strain Rates," Terra Tek, Presented at DASA Strategic Structures Long Range Planning Meeting, February 1971.

11. Brace, W. F., "Static Uniaxial Strain Behavior of 15 Rocks to 30 Kbar," Final Report, Massachusetts Institute of Technology, DASA 2561, November 1970.

12. Green, S. J., and R. D. Perkins, "Uniaxial Compression Tests at Strain Rates from 10^{-4} to 10^{4}/second on Three Geologic Materials," DASA 2119 and General Motors Materials and Structures Laboratory, Report No. MSL-68-6, April 1968.

13. Jones, A. H., and N. H. Froula, "Uniaxial Strain Behavior of Four Geologic Materials to 50 Kilobars," General Motors Corporation Materials and Structures Laboratory, MSL-68-19, March 1969 and DASA 2209.

14. Linde, R. K., and D. N. Schmidt, "Measuring the Submicrosecond Response of Shock Loaded Materials," Rev. Sci. Inst. 37 (1), (1966).

15. Rice, M. H., R. G. McQueen, and J. M. Walsh, "Compression of Solids by Strong Shock Waves," Solid State Physics, Vol. 6, F. Seitz and D. Turnbull, eds., Academic Press, New York, 1958.

16. Bethe, H. A., "The Theory of Shocks for an Arbitrary Equation of State," National Defense Research Committee of the Office of Scientific Research and Development, Publication OSRD No. 545, May 4, 1942.

17. Fowles, R., and R. F. Williams, J. Appl. Phys. 41, 360, 1970.

18. Cowperthwaite, M., and R. F. Williams, "Determination of Constitutive Relationships with Multiple Gages in Nondivergent Waves," J. Appl. Phys. 42, 456-462, 1971.

19. Ahrens, Thomas J., and V. G. Gregson, Jr., "Shock Compression of Crustal Rocks: Data for Quartz, Calcite, and Plagioclase Rocks," J. of Geophys. Res., 69, 4839-4874 (1964).

20. Seaman, Lynn, "SRI PUFF 3 Computer Code for Stress Wave Propagation," Technical Report, Stanford Research Institute, AFWL-TR-70-51, Sept. 1970.

21. Keough, D. D., "Procedure for Fabrication and Operation of Manganin Shock Pressure Gages," Final Report, Stanford Research Institute, AFWL-TR-68-57, 1968.

22. Barker, L. M. and R. E. Hollenbach, "Shock Wave Studies of PMMA, Fused Silica, and Sapphire," J. of Appl. Phys., 41, pp. 4208-4226, 1970.

23. Ahrens, T. J., J. T. Rosenberg, and M. H. Ruderman, "Dynamic Properties of Rocks," Final Report, Stanford Research Institute, DASA 1868, 1966.

24. Unpublished results, J. T. Rosenberg, D. Erlich, and R. Williams, Stanford Research Institute, 1971.

25. Chayes, F., "Composition of the Granites of Westerly and Bradford, Rhode Island," Am. Jour. Sci., 248, pp. 378-407, 1950.

26. Fairbairn, H. W., et al., "A Cooperative Investigation of Precision and Accuracy in Chemical, Spectrochemical and Modal Analysis of Silicate Rocks," Geological Survey Bulletin 980, 1951.

27. Simmons, Gene and W. F. Brace "Comparison of Static and Dynamic Measurements of Compressibility of Rocks," J. of Geophys. Res., 70, pp. 5649-5656, 1965.

28. Birch, Francis, "The Velocity of Compressional Waves in Rocks to 10 Kilobars, Part I," J. of Geophys. Res., 65, 1083-1101, 1960.

29. Brace, W. F., B. W. Baulding, and C. Scholz, "Dilatancy in the Fracture of Crystalline Rocks," J. Geophys. Res. 71, 3939-3953, 1966.

30. Peng, S. D., and A. M. Johnson, Private Communication from Professor A. M. Johnson, Dept. of Mineral Engineering and Geology, Stanford University.

31. Mogi, Kiyoo, "Some Precise Measurements of Fracture Strength of Rocks Under Uniform Compressive Stress," Felsmechanik and Ingenieurgeologue (Rock Mech. and Eng. Geol.), Vol. IV/1, 41-56 (1966).

32. Wackerle, Jerry, "Shock-Wave Compression of Quartz," J. Appl. Phys., 33, 922-937 (1962).

33. Gregson, V. G. Jr., S. J. Green, and W. M. Isbell, "The Effect of Material Strength on Wave Propagation in Rocks," Progress Report 19 and 20 prepared by Materials and Structures Laboratory, General Motors Corporation, for DASA under contract DA-49-146-XZ-544, Feb. 1970.

34. Brace, W. F. and R. J. Martin, III, "A Test of the Law of Effective Stress for Crystalline Rocks of Low Porosity," Int. J. Rock Mech. Min. Science, Vol. 5, 415-426 (1968).

35. LaMori, P. N., "Compressibility of Three Rocks, (A) Westerly Granite and Solenhofen Limestone to 40 Kbar and 300°C, (B) Cedar City Tonalite to 40 kbar at Room Temperature," DASA 2151, Battelle Memorial Institute, 1968.

36. Byerlee, J. D., "Static and Kinetic Friction of Granite at High Normal Stress," Int. J. Rock Mech. Min. Sci. Vol. 7, 577-582, 1970.